LA-UR-00-3329

Approved for public release;
distribution is unlimited.

Title: INTEGRATING A BILINEAR INTERPOLATION FUNCTION ACROSS QUADRILATERAL CELL BOUNDARIES

Author(s) Jerry S. Brock
Applied Physics Division

Submitted: August 2000

Photograph by Chris J. Lindberg

Los Alamos
NATIONAL LABORATORY

Form 836 (10/96)

Integrating a Bilinear Interpolation Function Across Quadrilateral Cell Boundaries

Jerry S. Brock, Applied Physics Division
Los Alamos National Laboratory, Los Alamos, NM 87545

Abstract

Computational models of particle dynamics often exchange solution data with discretized continuum-fields using interpolation functions. These particle methods require a series expansion of the interpolation function for two purposes: numerical analyses used to establish the models consistency and accuracy, and logical-coordinate evaluation used to locate particles within a grid. This report presents a new method of developing *discrete-expansions* for interpolation; they are similar to multi-variable expansions but, unlike a Taylor's series, discrete-expansions are valid throughout a discretized domain. Discrete-expansions are developed herein by parametrically integrating the interpolation function's total-differential between two particles located within separate, non-contiguous cells. Discrete-expansions are valid for numerical analyses since they acknowledge the functional dependence of interpolation and account for mapping discontinuities across cell boundaries. The use of discrete-expansions for logical-coordinate evaluation provides an algorithmically robust and computationally efficient particle localization method. Verification of this new method is demonstrated herein on a simple test problem.

Integrating a Bilinear Interpolation Function Across Quadrilateral Cell Boundaries

Introduction

Computational models of particle dynamics that are solved concurrently with discretized continuum-field equations are classified herein as either interactive or reactive particle methods. Interactive methods strongly couple the continuum and particle governing equations through the bilateral exchange of mass, momentum, and energy. These methods include models of liquid sprays [1-4], wall-film dynamics [5-8], bubble dynamics [9-13], smoke dispersion [14], and material-interface tracking [15,16]. In contrast, reactive particles simply respond to the entraining fluid, and their governing equations are weakly coupled to the field equations. Reactive methods include computing particle trajectories with a known velocity and additional physics, but their solution does not perturb the entraining fluid. These methods include models of atmospheric transport [17-24], porous-media diffusion [25-34], multi-phase dispersion [35-38], and transient mixing [39-41]. Both interactive and reactive methods often exchange solution data between continuum-fields and particles through interpolation functions. The focus of this research was on the role of one common interpolation function used within existing particle methods.

Particle methods use interpolation functions directly to evaluate terms in their governing equations. One simple reactive method is the marker or tracer-particle method, which advects a massless particle with an interpolated velocity [42-50]. These methods are used extensively for model diagnostics, solution visualization [51-53], free-surface tracking [54-59], and front tracking [60-66]. A Taylor's series of the velocity interpolation function, expanded from the particle's cell, is required to perform numerical analyses on these methods. Particle trajectories are often established using Runge-Kutta or predictor-corrector time-integration methods. The particle's advection velocity, the final velocity in these multi-step integration methods, may be evaluated in a neighboring cell. The expansion would then extend through multiple cells in the discretized domain. Derivatives of interpolation functions, however, are generally not continuous across cell boundaries and, therefore, a Taylor's series is not valid in this situation. An alternative expansion is required to complete numerical analyses for these and similar particle methods.

Particle methods also use interpolation functions indirectly to evaluate particle-grid connectivity data, which are required to exchange data between continuum-fields and particles. The connectivity data consist of the identity of the grid cell in which the particle resides and the particle's natural or logical-coordinate position vector relative to that cell. Particle localization establishes this data using cell-searching and logical-coordinate evaluation methods [67-72]. Cell-searching or guessing methods typically use the particle's logical coordinates to both direct and

halt the search. Evaluating these coordinates involves a transformation from global, physical-space to a local coordinate system [46,67,69,71-75]. If the logical coordinates are bound within known transformation limits, then the particle resides within the guessed cell. If these coordinates are unbound then another cell guess, directed by the unbound coordinates, and logical-coordinate evaluation are required. Particle methods are, thus, predicated on logical-coordinate evaluation methods which, as described below, are based on interpolation function expansions.

Particle methods, therefore, require the expansion of interpolation functions and utilize the expression in two different ways. Interpolation, mapping field data onto particles, requires direct substitution of the expansion into numerical analyses. In contrast, particle localization involves the inverse mapping of physical-space to logical-space coordinates. The mapping function then serves as both interpolation and spatial-transformation functions for isoparametric cells. The mathematical expression required for both numerical analysis and particle localization is identical and, therefore, the methods developed herein are valid for both purposes. The algorithmic requirements for inverse mapping, robustness and efficiency, are greater than those of algebraic manipulation required for interpolation. The remaining discussion and development, therefore, will emphasize interpolation expansions used for particle logical-coordinate evaluation.

The remaining discussion will also be restricted to the bilinear interpolation function as applied within quadrilateral cell geometries. These computational cells are one of the most commonly used geometries for two-dimensional discretization. When applied for spatial transformation, this bilinear mapping function is a linear combination of cell-vertex coordinate vectors weighted by basis functions. The basis functions are, however, non-linear with respect to the logical coordinates. The bilinear function is, therefore, a non-linear spatial-transformation function. A companion paper will document the following development applied to the linear interpolation function applied within two-dimensional triangular grid elements [76].

Existing logical-coordinate evaluation methods have been generalized in Reference [67] for various cell geometries. These methods were developed from a truncated, single-variable Taylor's series expansion of the interpolation function [46,67,69,71,72]. The expansion ignores the function's dependence on the cell-vertex coordinates and only considers the first-order dependence on the logical coordinates. The resulting system of equations is solved iteratively and requires the repeated evaluation and inversion of a Jacobian matrix. Logical-coordinate solutions using this technique are guaranteed if the particle resides within a guessed cell. Coordinate solutions may fail to exist, however, for cell geometries with non-linear transformations including bilinear interpolation; if the particle resides outside of a guessed cell and the grid is sufficiently distorted, the Jacobian matrix becomes singular and the iterative method fails to converge. This

solution method is, therefore, neither algorithmically robust nor computationally efficient. Two alternatives to the truncated, single-variable Taylor's series expansion are discussed below.

One obvious alternative to existing logical-coordinate evaluation methods would use a multi-variable Taylor's series. This expansion is appropriate for numerical analyses since it acknowledges the full functional dependence of interpolation. The expansion has a finite number of terms; for bilinear interpolation, only first and mixed second-order derivatives are non-zero. For particle localization, this expansion requires an iterative solution since the higher-order derivatives are scaled by unknown logical coordinates. In contrast to the existing methods, all derivatives in the multi-variable expansion are constant and computed only once, thereby providing a more efficient solution method. More importantly, the Jacobian matrix is evaluated with an arbitrarily fixed logical-coordinate vector. A bound coordinate vector may then be selected which guarantees a non-singular transformation matrix and, thus, a robust logical-coordinate evaluation method. All Taylor's series, however, are inherently invalid for expansions that extend beyond cell boundaries where interpolation derivatives are generally discontinuous.

Another alternative logical-coordinate evaluation method was recently proposed and demonstrated for three-dimensional hexahedral cells [73-75]. This method, developed using trilinear interpolation, considered the finite difference between two particles located in separate, non-contiguous cells. The resulting expression is termed herein a *discrete-expansion*; it is similar to a multi-variable Taylor's series expansion and, by accounting for discontinuous interpolation derivatives across cell boundaries, is valid throughout a discretized domain. The iterative solution of this new expression is both robust and efficient; its constant derivatives include a non-singular Jacobian matrix. This finite-difference solution is, therefore, appropriate for numerical analyses of particle methods and satisfies the algorithmic requirements for particle localization. The final form of this discrete-expansion, developed with much algebraic manipulation, was predominantly guided by intuition, however, and not physical relevance. Therefore, other possible discrete-expansions for interpolation functions were overlooked in recent reports [73-75].

This report presents a new method of developing discrete-expansions for interpolation. This development method integrates the interpolation function's total differential between two particles located within separate, non-contiguous grid cells. The integration is completed parametrically, and the resulting expressions are algebraically manipulated to obtain numerous discrete-expansions. Each of these multi-variable expressions may be used for numerical analyses since the total-differential method inherently accounts for discontinuous interpolation derivatives across cell boundaries. One of the new total-differential solutions is equivalent to the above finite-difference solution and, thus, satisfies the algorithmic requirements for logical-coordinate

evaluation. The total-differential method, therefore, represents a general solution technique, whose results are valid for both numerical analyses and localization for particle methods.

This report continues by parametrically integrating the bilinear interpolation function's total-differential. Application of the new discrete-expansions for numerical analyses or localization within particle methods is beyond the scope of this report. The utility of the total-differential solutions for these purposes, however, is discussed, and a summary concludes this report. Two appendices then present a test problem, which clearly demonstrates the new method's validity, and a similar development of discrete-expansions for one-dimensional line elements.

Bilinear Interpolation

Two-dimensional computational space is often discretized into non-orthogonal quadrilateral cells, particularly around complex geometries. A bilinear function is generally used within these cells for data interpolation and spatial transformation. Interpolation produces a continuous mapping of discrete field data, often located at cell-vertices, to any position in the cell. Spatial transformation involves mapping the cell geometry from a physical, $\overline{X} = (x, y)^T$, to a logical, $\overline{\xi} = (\xi, \eta)^T$, coordinate system; see Figure 1. While the physical coordinates of the cell-vertices are arbitrary, the quadrilateral's transformed coordinates are bound between zero and one; $\overline{\xi}$ is bound if $0 \le \xi \le 1$ and $0 \le \eta \le 1$. The bilinear function is dependent upon both $\overline{\xi}$ and the cell-vertex (cv) coordinate vector, $\overline{X}^{cv} = ({}^0\overline{X}, {}^1\overline{X}, {}^2\overline{X}, {}^3\overline{X})^T$, as presented in Equation 1.

$$\begin{aligned} \overline{X}(\overline{\xi}, \overline{X}^{cv}) = {} & (1-\xi)\,(1-\eta)\,{}^0\overline{X} \\ & + (\ \xi\ )\,(1-\eta)\,{}^1\overline{X} \\ & + (\ \xi\ )(\ \eta\ )\,{}^2\overline{X} \\ & + (1-\xi)(\ \eta\ )\,{}^3\overline{X} \end{aligned} \tag{1}$$

Bilinear interpolation is linear with respect to the cell-vertex vector, $\overline{X}^{cv}$, but non-linear with respect to the logical coordinates, $\overline{\xi}$. Interpolated data fields, produced by the application of Equation 1 in each grid cell, are continuous along the common boundaries of adjoining cells.

Total Differential

Using the bilinear function, $\overline{X}(\overline{\xi}, \overline{X}^{cv})$, the objective is to establish a relationship between the finite change of the physical coordinates, $\Delta\overline{X}$, the logical coordinates, $\Delta\overline{\xi}$, and the cell-vertex coordinates, $\Delta\overline{X}^{cv}$. The bilinear function's total-differential provides a relationship between infinitesimal changes of these coordinate vectors, $d\overline{X} = f(d\overline{\xi}, d\overline{X}^{cv})$, as presented in Equation 2.

$$d\bar{X} = \frac{\partial \bar{X}(\bar{\xi}, \bar{X}^{cv})}{\partial \bar{\xi}} d\bar{\xi} + \frac{\partial \bar{X}(\bar{\xi}, \bar{X}^{cv})}{\partial \bar{X}^{cv}} d\bar{X}^{cv} \tag{2}$$

Integration of this expression between particle end-states will provide the desired relationship, $\Delta\bar{X} = f(\Delta\bar{\xi}, \Delta\bar{X}^{cv})$, which represents a discrete-expansion for interpolation.

Logical Coordinate Derivative

The bilinear function's total-differential includes two interpolation derivatives or transformation matrices that are scaled by differential coordinate vectors. The first derivative in Equation 2 represents a coordinate-transformation or Jacobian matrix, $J = \partial\bar{X}/\partial\bar{\xi}$. The Jacobian matrix structure is defined in Equation 3 for a two-dimensional transformation.

$$\left[\frac{\partial \bar{X}}{\partial \bar{\xi}}\right]_{2x2} = \left[\frac{\partial \bar{X}}{\partial \xi} \; \frac{\partial \bar{X}}{\partial \eta}\right]_{2x2} = \begin{bmatrix} \frac{\partial x}{\partial \xi} & \frac{\partial x}{\partial \eta} \\ \frac{\partial y}{\partial \xi} & \frac{\partial y}{\partial \eta} \end{bmatrix}_{2x2} \tag{3}$$

The size of the square Jacobian matrix is determined by the number of spatial coordinates. Elements of this coordinate-transformation matrix are most easily expressed as column vectors. The derivatives $\partial\bar{X}/\partial\xi$ and $\partial\bar{X}/\partial\eta$ for bilinear interpolation are presented in Equations 4 and 5.

$$\begin{aligned} \frac{\partial \bar{X}}{\partial \xi}(\eta, \bar{X}^{cv}) = & -(1-\eta)\,{}^{0}\bar{X} \\ & +(1-\eta)\,{}^{1}\bar{X} \\ & +(\;\eta\;)\,{}^{2}\bar{X} \\ & -(\;\eta\;)\,{}^{3}\bar{X} \end{aligned} \tag{4}$$

$$\begin{aligned} \frac{\partial \bar{X}}{\partial \eta}(\xi, \bar{X}^{cv}) = & -(1-\xi)\,{}^{0}\bar{X} \\ & -(\;\xi\;)\,{}^{1}\bar{X} \\ & +(\;\xi\;)\,{}^{2}\bar{X} \\ & +(1-\xi)\,{}^{3}\bar{X} \end{aligned} \tag{5}$$

The above derivatives are similar to the original bilinear function; each column vector in the Jacobian matrix is a linear combination of cell-vertex vectors weighted by basis functions. In contrast to Equation 1, the basis functions in Equations 4 and 5 are linear with respect to the

logical coordinates since they are dependent on only one element of $\bar{\xi}$. The Jacobian matrix for bilinear interpolation, which combines these column vectors, is, therefore, a linear function with respect to both the logical-coordinate and cell-vertex coordinate vectors: $J = \partial\bar{X}(\bar{\xi}, \bar{X}^{cv})/\partial\bar{\xi}$.

Cell-Vertex Coordinate Derivative

The second derivative in the bilinear interpolation function's total-differential, Equation 2, represents a geometry-transformation matrix. The matrix structure of $\partial\bar{X}/\partial\bar{X}^{cv}$, the cell-vertex coordinate derivative, is defined in Equation 6 for a two-dimensional transformation.

$$\left[\frac{\partial\bar{X}}{\partial\bar{X}^{cv}}\right]_{2x8} = \left[\frac{\partial\bar{X}}{\partial^0\bar{X}} \; \frac{\partial\bar{X}}{\partial^1\bar{X}} \; \frac{\partial\bar{X}}{\partial^2\bar{X}} \; \frac{\partial\bar{X}}{\partial^3\bar{X}}\right]_{2x8} \tag{6}$$

The geometry-transformation matrix is non-square. The number of rows and columns in this matrix are determined by the problem dimension size and the number of elements within the cell-vertex coordinate vector, $\bar{X}^{cv}$, respectfully. The size of $\bar{X}^{cv}$ is the problem dimension size multiplied by the number of cell vertices. As presented, the geometry-transformation matrix may be partitioned into sub-matrices, each of which is associated with a single cell-vertex position. One sub-matrix, associated with any cell-vertex number 'v', is presented in Equation 7.

$$\left[\frac{\partial\bar{X}}{\partial^v\bar{X}}\right]_{2x2} = \left[\frac{\partial\bar{X}}{\partial^v x} \; \frac{\partial\bar{X}}{\partial^v y}\right]_{2x2} = \left[\begin{matrix}\frac{\partial x}{\partial^v x} & \frac{\partial x}{\partial^v y} \\ \frac{\partial y}{\partial^v x} & \frac{\partial y}{\partial^v y}\end{matrix}\right]_{2x2} \tag{7}$$

The square structure and size of each partition within the geometry-transformation matrix are similar to Equation 3, the Jacobian matrix. In contrast to the full Jacobian matrix, the geometry transformation's sub-matrices are diagonal as presented in Equation 8.

$$\left[\frac{\partial\bar{X}}{\partial^v\bar{X}}\right]_{2x2} = \left[\begin{matrix}\frac{\partial x}{\partial^v x} & 0 \\ 0 & \frac{\partial y}{\partial^v y}\end{matrix}\right]_{2x2} \tag{8}$$

The elements of the sub-matrices within $\partial\bar{X}/\partial\bar{X}^{cv}$ are most easily presented for each cell-vertex position. These sub-matrix elements, $\partial x/\partial^v x$ and $\partial y/\partial^v y$, are identical to the basis functions used within bilinear interpolation as presented in Equation 9.

$$\begin{aligned}
\frac{\partial x}{\partial^0 x}(\bar{\xi}) &= \frac{\partial y}{\partial^0 y}(\bar{\xi}) = (1-\xi)\,(1-\eta) \\
\frac{\partial x}{\partial^1 x}(\bar{\xi}) &= \frac{\partial y}{\partial^1 y}(\bar{\xi}) = (\ \ \xi\ \ )\,(1-\eta) \\
\frac{\partial x}{\partial^2 x}(\bar{\xi}) &= \frac{\partial y}{\partial^2 y}(\bar{\xi}) = (\ \ \xi\ \ )\,(\ \ \eta\ \ ) \\
\frac{\partial x}{\partial^3 x}(\bar{\xi}) &= \frac{\partial y}{\partial^3 y}(\bar{\xi}) = (1-\xi)\,(\ \ \eta\ \ )
\end{aligned} \tag{9}$$

For each cell-vertex vector, the derivatives with respect to both ${}^{v}x$ and ${}^{v}y$ are identical. Each geometry-transformation sub-matrix may then be defined, but not shown here, as an identity matrix scaled by an interpolation basis function. The derivatives in Equation 9 are non-linear with respect to the logical coordinates since they are multiples of every element within the $\bar{\xi}$ vector. In contrast, since bilinear interpolation is linear with respect to $\bar{X}^{cv}$, the geometry-transformation matrix is not a function of the cell-vertex coordinate vector: $\partial\bar{X}(\bar{\xi})/\partial\bar{X}^{cv}$.

Considering the functionality of both the Jacobian and geometry-transformation matrices, the bilinear interpolation function's simplified total-differential is presented in Equation 10.

$$d\bar{X} = \frac{\partial\bar{X}}{\partial\bar{\xi}}(\bar{\xi}, \bar{X}^{cv})\, d\bar{\xi} + \frac{\partial\bar{X}}{\partial\bar{X}^{cv}}(\bar{\xi})\, d\bar{X}^{cv} \tag{10}$$

Integration Method

The objective is to integrate the bilinear function's total-differential, Equation 10, to obtain a discrete-expansion for interpolation: $\Delta\bar{X} = f(\Delta\bar{\xi}, \Delta\bar{X}^{cv})$. The limits of integration are two particles located in separate cells: State 1, $\bar{X}_1 = \bar{X}(\bar{\xi}_1, \bar{X}_1^{cv})$, and State 2, $\bar{X}_2 = \bar{X}(\bar{\xi}_2, \bar{X}_2^{cv})$. The computational sub-domains in which the particles reside are not desired to be connected in physical-space; see Figure 2. Integration of the total-differential is represented in Equation 11.

$$\int_1^2 d\bar{X} = \int_1^2 \frac{\partial\bar{X}}{\partial\bar{\xi}}(\bar{\xi}, \bar{X}^{cv})\, d\bar{\xi} + \int_1^2 \frac{\partial\bar{X}}{\partial\bar{X}^{cv}}(\bar{\xi})\, d\bar{X}^{cv} \tag{11}$$

The linearity and continuity of the derivatives in the total-differential affect the integration process used to obtain a discrete-expansion. The linearity of the interpolation derivatives determines the complexity of the integration process. For bilinear interpolation, the coordinate-transformation matrix, $\partial\bar{X}(\bar{\xi}, \bar{X}^{cv})/\partial\bar{\xi}$, is linear with respect to both $\bar{\xi}$ and $\bar{X}^{cv}$. The geometry-transformation matrix, $\partial\bar{X}(\bar{\xi})/\partial\bar{X}^{cv}$, while not a function of $\bar{X}^{cv}$, is non-linear with respect to $\bar{\xi}$.

More importantly, continuity of the interpolation derivatives is required for the total-differential to be valid within a specified region. Solution of Equation 11 in a single cell is straightforward; the interpolation derivatives are guaranteed to be continuous in this region. In contrast, if the limits of integration cross a cell boundary, solution of Equation 11 is more complex.

Solution of Equation 11 between particles located in separate but adjoining cells involves integrating the interpolation function's total-differential through two unique coordinate systems. While the form of the interpolation expression is identical for each cell, the two functions are different; they have distinct cell-vertex coordinate vectors. Along their common cell-edge, the two interpolation functions are continuous but their derivatives are generally discontinuous. Therefore, for any integration pathline that crosses a cell boundary, the interpolation derivatives are not continuous, and the total-differential is not valid between these particle positions. Discrete-expansions can then only be obtained from Equation 11 if the integration pathline is partitioned or if the integration coordinate-space is appropriately parameterized.

An integration pathline that passes between adjoining cells may be partitioned into two line-segments, each defined within a separate coordinate system. The interpolation derivatives are guaranteed to be continuous throughout each computational sub-domain. The integrals within Equation 11 are similarly partitioned into cell-based segments along which the total-differential is valid. Integration along this two-segment pathline would then proceed within the first cell from State 1 to the cell boundary, then within the second cell from the common cell-edge to State 2. While this integration procedure represents a valid method of solution for Equation 11, it is algorithmically complex and computationally expensive. Furthermore, when particle end-states are located within non-contiguous grid cells, partition of the integration pathline through the multiple intermediary computational sub-domains is prohibitively complex and expensive.

Parameterization

Alternatively, the coordinate-space between the limits of integration can be parameterized. Solution of Equation 11 across boundaries of adjoining cells fails in general because it requires integrating unique interpolation functions through separate coordinate systems. Parameterization removes the concept of multiple coordinate systems by creating a single coordinate-space between any two particle positions. The form of the parameterization function is arbitrary, this research used a linear function, however, it must be continuously differentiable since it is embedded within the interpolation function whose derivatives appear within the total-differential. The parameterized interpolation derivatives are then guaranteed to be continuous along the entire integration pathline. A parameterized total-differential may then be integrated directly without requiring partition of the integration pathline into cell-based line-segments.

Parameterization involves creating a new coordinate-space between two particle states. Since particle states are a collection of physical, logical, and cell-vertex coordinates, each of these vectors must be parameterized. A simple, linear parameterization technique using the variable 's', where $0 \le s \le 1$, was selected in this research. The parameterized coordinates, $\overline{X}(s)$, $\overline{\xi}(s)$ and $\overline{X}^{cv}(s)$, then vary linearly along any integration pathline between particle positions. The limits of integration for the parameterized total-differential are transformed from particle state-variables into the bounding limits of the variable 's'. Integration of the parameterized total-differential for bilinear interpolation, with appropriate limits of integration, is represented in Equation 12.

$$\int_0^1 \frac{\partial \overline{X}(s)}{\partial s}\, ds = \int_0^1 \frac{\partial \overline{X}}{\partial \overline{\xi}}(\overline{\xi}(s), \overline{X}^{cv}(s)) \frac{\partial \overline{\xi}(s)}{\partial s}\, ds + \int_0^1 \frac{\partial \overline{X}}{\partial \overline{X}^{cv}}(\overline{\xi}(s)) \frac{\partial \overline{X}^{cv}(s)}{\partial s}\, ds \qquad (12)$$

The solution of Equation 12 requires a path of integration. While the parameterization function does not prescribe the shape of the integration pathline, it does define the parameterization variable's behavior along any path between two particles. The only restriction on the limits of integration are that the end-state variables form a consistent set of coordinates as described by the interpolation function: $\overline{X} = \overline{X}(\overline{\xi}, \overline{X}^{cv})$. Parameterization transforms the multi-variable integration process, involving each element within the $\overline{\xi}$ and $\overline{X}^{cv}$ vectors, to a simple one-dimensional problem with respect to the parameterization variable. Cell-based coordinate systems are then irrelevant, and the limits of integration may be any two particle positions within the discretized domain. The integration pathline can then be defined between any two computational sub-domains, including any two non-contiguous grid cells.

The remaining solution process for Equation 12 requires definition of a specific pathline of integration between the particle States 1 and 2. An integration pathline for the parameterized total-differential traverses through the plane defined by the logical-coordinate and cell-vertex coordinate vectors, $\overline{\xi}$ and $\overline{X}^{cv}$. These two vectors are the arguments of the bilinear function as defined for spatial transformation: $\overline{X} = \overline{X}(\overline{\xi}, \overline{X}^{cv})$. Three unique integration pathlines described within the $(\overline{\xi}, \overline{X}^{cv})$ plane were selected by this research to solve Equation 12: direct, upper-step, and lower-step integration pathlines. Solution of Equation 12 using each of these pathlines produces many unique but equally valid discrete-expansions for interpolation.

Direct Integration Pathline

The first integration pathline used to solve Equation 12 is a straight or direct line between particle States 1 and 2; see Figure 3. The parametrized coordinates vary linearly along this direct pathline, and reduce to the particle end-state coordinates at the bounding limits of integration. These parameterized coordinates are presented in Equation 13.

$$\begin{aligned} \text{State 1} \rightarrow \text{State 2} \quad : \quad \overline{X}(s) &= (1-s)\,\overline{X}_1 + (s)\,\overline{X}_2 \\ \overline{\xi}(s) &= (1-s)\,\overline{\xi}_1 + (s)\,\overline{\xi}_2 \\ \overline{X}^{cv}(s) &= (1-s)\,\overline{X}_1^{cv} + (s)\,\overline{X}_2^{cv} \end{aligned} \tag{13}$$

Solution of Equation 12 along the direct integration pathline is represented in Equation 14, where the interpolation derivatives are appropriately labeled.

$$\begin{aligned} \int_0^1 \frac{\partial \overline{X}(s)}{\partial s}\bigg|_{1\rightarrow 2} ds &= \int_0^1 \frac{\partial \overline{X}}{\partial \overline{\xi}}(\overline{\xi}(s), \overline{X}^{cv}(s))\bigg|_{1\rightarrow 2} \frac{\partial \overline{\xi}(s)}{\partial s}\bigg|_{1\rightarrow 2} ds \\ &+ \int_0^1 \frac{\partial \overline{X}}{\partial \overline{X}^{cv}}(\overline{\xi}(s))\bigg|_{1\rightarrow 2} \frac{\partial \overline{X}^{cv}(s)}{\partial s}\bigg|_{1\rightarrow 2} ds \end{aligned} \tag{14}$$

Since the parameterized coordinates are linear functions, their derivatives are constant finite-difference vectors: $\partial \overline{X}(s)/\partial s = \Delta \overline{X}$, $\partial \overline{\xi}(s)/\partial s = \Delta \overline{\xi}$ and $\partial \overline{X}^{cv}(s)/\partial s = \Delta \overline{X}^{cv}$. These difference vectors are defined between particle States 1 and 2: $\Delta \overline{X} = \overline{X}_2 - \overline{X}_1$, $\Delta \overline{\xi} = \overline{\xi}_2 - \overline{\xi}_1$, and $\Delta \overline{X}^{cv} = \overline{X}_2^{cv} - \overline{X}_1^{cv}$. Integration of the parameterized total-differential along the direct pathline can then be simplified as presented in Equation 15.

$$\int_0^1 \Delta \overline{X}\, ds = \int_0^1 \frac{\partial \overline{X}}{\partial \overline{\xi}}(\overline{\xi}(s), \overline{X}^{cv}(s))\bigg|_{1\rightarrow 2} \Delta \overline{\xi}\, ds + \int_0^1 \frac{\partial \overline{X}}{\partial \overline{X}^{cv}}(\overline{\xi}(s))\bigg|_{1\rightarrow 2} \Delta \overline{X}^{cv}\, ds \tag{15}$$

The parameterized transformation matrices, $\partial \overline{X}(\overline{\xi}(s), \overline{X}^{cv}(s))/\partial \overline{\xi}$ and $\partial \overline{X}(\overline{\xi}(s))/\partial \overline{X}^{cv}$, in Equation 15 are formed by substituting $\overline{\xi}(s)$ and $\overline{X}^{cv}(s)$ from Equation 13 into Equations 4, 5, and 9. These derivatives are non-linear with respect the parameterization variable, and include constant particle end-state coordinates: $\overline{\xi}_1$, $\overline{\xi}_2$, $\overline{X}_1^{cv}$ and $\overline{X}_2^{cv}$. Solution of Equation 15 is then straightforward, and many discrete-expansions may be obtained. The two discrete-expansions most easily obtained using the direct integration pathline are presented in Equation 16.

$$\begin{aligned} \Delta \overline{X} &= \frac{\partial \overline{X}}{\partial \overline{\xi}}(\hat{\overline{\xi}}, \hat{\overline{X}}^{cv})\,\Delta \overline{\xi} + \frac{\partial \overline{X}}{\partial \overline{X}^{cv}}(\hat{\overline{\xi}})\,\Delta \overline{X}^{cv} + \frac{1}{4}\frac{\partial^2 \overline{X}}{\partial \xi \partial \eta}(\Delta \overline{X}^{cv})\,\Delta \xi\,\Delta \eta \\ \Delta \overline{X} &= \frac{1}{2}\frac{\partial \overline{X}}{\partial \overline{\xi}}(\overline{\xi}_1, \overline{X}_1^{cv})\,\Delta \overline{\xi} + \frac{1}{2}\frac{\partial \overline{X}}{\partial \overline{X}^{cv}}(\overline{\xi}_1)\,\Delta \overline{X}^{cv} \\ &+ \frac{1}{2}\frac{\partial \overline{X}}{\partial \overline{\xi}}(\overline{\xi}_2, \overline{X}_2^{cv})\,\Delta \overline{\xi} + \frac{1}{2}\frac{\partial \overline{X}}{\partial \overline{X}^{cv}}(\overline{\xi}_2)\,\Delta \overline{X}^{cv} - \frac{1}{2}\frac{\partial^2 \overline{X}}{\partial \xi \partial \eta}(\Delta \overline{X}^{cv})\,\Delta \xi\,\Delta \eta \end{aligned} \tag{16}$$

The discrete-expansions in Equation 16 are combinations of transformation matrices and a higher-order interpolation derivative. Evaluation of the coordinate and geometry transformation matrices is easily visualized using Figure 3. Arguments for these first-order derivatives are either particle end-state coordinates or their averages: $\hat{\bar{\xi}} = (\bar{\xi}_1 + \bar{\xi}_2)/2$ and $\hat{\bar{X}}^{cv} = (\bar{X}_1^{cv} + \bar{X}_2^{cv})/2$. In contrast, the argument for the higher-order derivative is the difference in cell-vertex coordinates, $\Delta\bar{X}^{cv}$. The transformation matrices are scaled by finite-difference vectors of the logical-coordinate and cell-vertex coordinate variables: $\Delta\bar{\xi}$ and $\Delta\bar{X}^{cv}$. The second-order interpolation derivative, the vector $\partial^2\bar{X}/\partial\xi\partial\eta$, is multiplied by two scalar finite-differences defined from the elements in the two-dimensional logical-coordinate vector: $\Delta\xi$ and $\Delta\eta$.

Upper-Step Integration Pathline

The second integration pathline used to solve Equation 12 is comprised of two line-segments between particle States 1 and 2. The first pathline segment is a line of constant $\bar{\xi}$ from State 1 to State A; see Figure 3. State A is a collection of logical-coordinates defined at State 1 and cell-vertex coordinates defined at State 2: $\bar{X}_A = \bar{X}(\bar{\xi}_1, \bar{X}_2^{cv})$. The second pathline segment is a line of constant $\bar{X}^{cv}$ from State A to State 2. These two pathline segments form an upper-step within the $(\bar{\xi}, \bar{X}^{cv})$ plane. The parametrized coordinates vary linearly along each segment of the upper-step pathline, and reduce to the particle end-state coordinates at the bounding limits of integration. These parameterized coordinates are presented in Equations 17 and 18.

$$\begin{aligned}
\text{State 1} \rightarrow \text{State A} \quad : \quad \bar{X}(s) &= (1-s)\,\bar{X}_1 + (s)\,\bar{X}_A \\
\bar{\xi}(s) &= (1-s)\,\bar{\xi}_1 + (s)\,\bar{\xi}_A \;;\; \bar{\xi}_A = \bar{\xi}_1 \\
&= \bar{\xi}_1 \\
\bar{X}^{cv}(s) &= (1-s)\,\bar{X}_1^{cv} + (s)\,\bar{X}_A^{cv} \;;\; \bar{X}_A^{cv} = \bar{X}_2^{cv} \\
&= (1-s)\,\bar{X}_1^{cv} + (s)\,\bar{X}_2^{cv}
\end{aligned} \tag{17}$$

$$\begin{aligned}
\text{State A} \rightarrow \text{State 2} \quad : \quad \bar{X}(s) &= (1-s)\,\bar{X}_A + (s)\,\bar{X}_2 \\
\bar{\xi}(s) &= (1-s)\,\bar{\xi}_A + (s)\,\bar{\xi}_2 \;;\; \bar{\xi}_A = \bar{\xi}_1 \\
&= (1-s)\,\bar{\xi}_1 + (s)\,\bar{\xi}_2 \\
\bar{X}^{cv}(s) &= (1-s)\,\bar{X}_A^{cv} + (s)\,\bar{X}_2^{cv} \;;\; \bar{X}_A^{cv} = \bar{X}_2^{cv} \\
&= \bar{X}_2^{cv}
\end{aligned} \tag{18}$$

The upper-step integration pathline does not constitute cell-based partition of the original, non-parameterized total-differential. Instead, the upper-step pathline is used to integrate the parameterized total-differential, which is not dependent upon cell-based coordinate systems.

Recall that a parameterized total-differential may be integrated between any two particles within the discretized domain, including particles that occupy non-contiguous cells. State A simply represents any position along any integration pathline within the parameterized coordinate-space, which is the $(\bar{\xi}, \bar{X}^{cv})$ plane when interpolation is used for spatial-transformation. Integration of the non-parameterized total-differential, Equation 11, can be rewritten to simulate the upper-step integration pathline as presented in Equation 19.

$$\begin{aligned} \int_1^A d\bar{X} + \int_A^2 d\bar{X} = & \int_1^A \frac{\partial \bar{X}}{\partial \bar{\xi}}(\bar{\xi}, \bar{X}^{cv})\, d\bar{\xi} + \int_A^2 \frac{\partial \bar{X}}{\partial \bar{\xi}}(\bar{\xi}, \bar{X}^{cv})\, d\bar{\xi} \\ & + \int_1^A \frac{\partial \bar{X}}{\partial \bar{X}^{cv}}(\bar{\xi})\, d\bar{X}^{cv} + \int_A^2 \frac{\partial \bar{X}}{\partial \bar{X}^{cv}}(\bar{\xi})\, d\bar{X}^{cv} \end{aligned} \tag{19}$$

Using the upper-step pathline, integration of the parameterized version of Equation 19 is represented in Equation 20, where the interpolation derivatives are appropriately labeled.

$$\begin{aligned} & \int_0^1 \frac{\partial \bar{X}(s)}{\partial s}\bigg|_{1\to A} ds + \int_0^1 \frac{\partial \bar{X}(s)}{\partial s}\bigg|_{A\to 2} ds = \\ & + \int_0^1 \frac{\partial \bar{X}}{\partial \bar{\xi}}(\bar{\xi}(s), \bar{X}^{cv}(s))\bigg|_{1\to A} \frac{\partial \bar{\xi}(s)}{\partial s}\bigg|_{1\to A} ds + \int_0^1 \frac{\partial \bar{X}}{\partial \bar{\xi}}(\bar{\xi}(s), \bar{X}^{cv}(s))\bigg|_{A\to 2} \frac{\partial \bar{\xi}(s)}{\partial s}\bigg|_{A\to 2} ds \\ & + \int_0^1 \frac{\partial \bar{X}}{\partial \bar{X}^{cv}}(\bar{\xi}(s))\bigg|_{1\to A} \frac{\partial \bar{X}^{cv}(s)}{\partial s}\bigg|_{1\to A} ds + \int_0^1 \frac{\partial \bar{X}}{\partial \bar{X}^{cv}}(\bar{\xi}(s))\bigg|_{A\to 2} \frac{\partial \bar{X}^{cv}(s)}{\partial s}\bigg|_{A\to 2} ds \end{aligned} \tag{20}$$

Along each segment of the upper-step integration pathline, one of the parameterized coordinates is held constant while the other coordinates vary linearly between particle states. Derivatives of the parameterized coordinates are then either the null vector or a finite-difference vector. Along the first pathline segment from State 1 to State A, where $\bar{\xi}$ is held constant, $\partial\bar{\xi}(s)/\partial s = 0$ and $\partial\bar{X}^{cv}(s)/\partial s = \Delta\bar{X}^{cv}$. Alternately, along the second pathline segment from State A to State 2, where $\bar{X}^{cv}$ is held constant, $\partial\bar{\xi}(s)/\partial s = \Delta\bar{\xi}$ and $\partial\bar{X}^{cv}(s)/\partial s = 0$. Along the entire upper-step pathline $\partial\bar{X}(s)/\partial s = \Delta\bar{X}$. Integration of the parameterized total-differential along the upper-step pathline can then be simplified as presented in Equation 21.

$$\int_0^1 \Delta\bar{X}\, ds = \int_0^1 \frac{\partial \bar{X}}{\partial \bar{\xi}}(\bar{\xi}(s), \bar{X}^{cv}(s))\bigg|_{A\to 2} \Delta\bar{\xi}\, ds + \int_0^1 \frac{\partial \bar{X}}{\partial \bar{X}^{cv}}(\bar{\xi}(s))\bigg|_{1\to A} \Delta\bar{X}^{cv}\, ds \tag{21}$$

The parameterized transformation matrices in Equation 21 are formed by substituting $\bar{\xi}(s)$ and $\bar{X}^{cv}(s)$ from Equations 17 and 18 into Equations 4, 5, and 9. These interpolation

derivatives, which are products of linear parameterized coordinates, are more simple than those defined along the direct integration pathline. Since one parameterized coordinate is fixed along each of the upper-step pathline segments, the degree of non-linearity is one order lower than those defined along the direct integration pathline. Solution of Equation 21 is then straightforward, and many discrete-expansions may be obtained. The three discrete-expansions most easily obtained using the upper-step integration pathline are presented in Equation 22.

$$\begin{aligned}
\Delta\bar{X} &= \frac{\partial\bar{X}}{\partial\bar{\xi}}(\hat{\bar{\xi}}, \bar{X}_2^{cv})\,\Delta\bar{\xi} + \frac{\partial\bar{X}}{\partial\bar{X}^{cv}}(\bar{\xi}_1)\,\Delta\bar{X}^{cv} \\
\Delta\bar{X} &= \frac{\partial\bar{X}}{\partial\bar{\xi}}(\bar{\xi}_1, \bar{X}_2^{cv})\,\Delta\bar{\xi} + \frac{\partial^2\bar{X}}{\partial\xi\partial\eta}(\bar{X}_2^{cv})\,\Delta\xi\,\Delta\eta + \frac{\partial\bar{X}}{\partial\bar{X}^{cv}}(\bar{\xi}_1)\,\Delta\bar{X}^{cv} \qquad (22) \\
\Delta\bar{X} &= \frac{\partial\bar{X}}{\partial\bar{\xi}}(\bar{\xi}_2, \bar{X}_2^{cv})\,\Delta\bar{\xi} - \frac{\partial^2\bar{X}}{\partial\xi\partial\eta}(\bar{X}_2^{cv})\,\Delta\xi\,\Delta\eta + \frac{\partial\bar{X}}{\partial\bar{X}^{cv}}(\bar{\xi}_1)\,\Delta\bar{X}^{cv}
\end{aligned}$$

The discrete-expansions in Equation 22 are similar to those in Equation 16; they are combinations of transformation matrices and a higher-order derivative. Within Equation 22, the cell-vertex arguments for the interpolation derivatives with respect to $\bar{\xi}$, both $\partial\bar{X}/\partial\bar{\xi}$ and $\partial^2\bar{X}/\partial\xi\partial\eta$, are fixed at $\bar{X}_2^{cv}$; the logical-coordinates vary along the pathline segment where $\bar{X}^{cv}$ is fixed at State 2. Similarly, within Equation 22 the logical-coordinate argument for the geometry-transformation matrix, $\partial\bar{X}/\partial\bar{X}^{cv}$, is fixed at $\bar{\xi}_1$; the cell-vertex coordinates vary along the pathline segment where $\bar{\xi}$ is fixed at State 1. In contrast, the logical-coordinates used within the coordinate-transformation matrix, $\partial\bar{X}/\partial\bar{\xi}$, can be either particle end-state coordinates or their averages, $\hat{\bar{\xi}}$. The second-order derivative is present in the expansions only when the two particle end-state coordinates, $\bar{\xi}_1$ and $\bar{\xi}_2$, appear within $\partial\bar{X}/\partial\bar{\xi}$.

The second expression within Equation 22 is the two-dimensional equivalent of the discrete-expansion obtained using the finite-difference method [73-75]. Therefore, the new total-differential and the existing finite-difference methods of developing discrete-expansions produce identical results for similar computational cell geometries; bilinear interpolation defined within quadrilateral cells is a subset of the trilinear function defined within hexahedral cell geometries.

Lower-Step Integration Pathline

The third integration pathline used to solve Equation 12 is similar to the upper-step pathline. This final pathline alternative is also comprised of two line-segments between particle States 1 and 2. The first pathline segment is a line of constant $\bar{X}^{cv}$ from State 1 to State B; see Figure 3. State B is a collection of logical-coordinates defined at State 2 and cell-vertex

coordinates defined at State 1: $\bar{X}_B = \bar{X}(\bar{\xi}_2, \bar{X}_1^{cv})$. The second pathline segment is a line of constant $\bar{\xi}$ from State B to State 2. These two pathline segments form a lower-step within the $(\bar{\xi}, \bar{X}^{cv})$ plane. These parameterized coordinates are presented in Equations 23 and 24.

$$\begin{aligned}
\text{State 1} \rightarrow \text{State B} \quad : \quad \bar{X}(s) &= (1-s)\,\bar{X}_1 + (s)\,\bar{X}_B \\
\bar{\xi}(s) &= (1-s)\,\bar{\xi}_1 + (s)\,\bar{\xi}_B \;;\; \bar{\xi}_B = \bar{\xi}_2 \\
&= (1-s)\,\bar{\xi}_1 + (s)\,\bar{\xi}_2 \\
\bar{X}^{cv}(s) &= (1-s)\,\bar{X}_1^{cv} + (s)\,\bar{X}_B^{cv} \;;\; \bar{X}_B^{cv} = \bar{X}_1^{cv} \\
&= \bar{X}_1^{cv}
\end{aligned} \tag{23}$$

$$\begin{aligned}
\text{State B} \rightarrow \text{State 2} \quad : \quad \bar{X}(s) &= (1-s)\,\bar{X}_B + (s)\,\bar{X}_2 \\
\bar{\xi}(s) &= (1-s)\,\bar{\xi}_B + (s)\,\bar{\xi}_2 \;;\; \bar{\xi}_B = \bar{\xi}_2 \\
&= \bar{\xi}_2 \\
\bar{X}^{cv}(s) &= (1-s)\,\bar{X}_B^{cv} + (s)\,\bar{X}_2^{cv} \;;\; \bar{X}_B^{cv} = \bar{X}_1^{cv} \\
&= (1-s)\,\bar{X}_1^{cv} + (s)\,\bar{X}_2^{cv}
\end{aligned} \tag{24}$$

Integration of the non-parameterized total-differential, Equation 11, can be rewritten to simulate the lower-step integration pathline as presented in Equation 25.

$$\begin{aligned}
\int_1^B d\bar{X} + \int_B^2 d\bar{X} &= \int_1^B \frac{\partial \bar{X}}{\partial \bar{\xi}}(\bar{\xi}, \bar{X}^{cv})\, d\bar{\xi} + \int_B^2 \frac{\partial \bar{X}}{\partial \bar{\xi}}(\bar{\xi}, \bar{X}^{cv})\, d\bar{\xi} \\
&+ \int_1^B \frac{\partial \bar{X}}{\partial \bar{X}^{cv}}(\bar{\xi})\, d\bar{X}^{cv} + \int_B^2 \frac{\partial \bar{X}}{\partial \bar{X}^{cv}}(\bar{\xi})\, d\bar{X}^{cv}
\end{aligned} \tag{25}$$

Using the lower-step pathline, integration of the parameterized version of Equation 25 is represented in Equation 26, where the interpolation derivatives are appropriately labeled.

$$\begin{aligned}
&\int_0^1 \left.\frac{\partial \bar{X}(s)}{\partial s}\right|_{1\rightarrow B} ds + \int_0^1 \left.\frac{\partial \bar{X}(s)}{\partial s}\right|_{B\rightarrow 2} ds = \\
&+ \int_0^1 \left.\frac{\partial \bar{X}}{\partial \bar{\xi}}(\bar{\xi}(s), \bar{X}^{cv}(s))\right|_{1\rightarrow B} \left.\frac{\partial \bar{\xi}(s)}{\partial s}\right|_{1\rightarrow B} ds + \int_0^1 \left.\frac{\partial \bar{X}}{\partial \bar{\xi}}(\bar{\xi}(s), \bar{X}^{cv}(s))\right|_{B\rightarrow 2} \left.\frac{\partial \bar{\xi}(s)}{\partial s}\right|_{B\rightarrow 2} ds \\
&+ \int_0^1 \left.\frac{\partial \bar{X}}{\partial \bar{X}^{cv}}(\bar{\xi}(s))\right|_{1\rightarrow B} \left.\frac{\partial \bar{X}^{cv}(s)}{\partial s}\right|_{1\rightarrow B} ds + \int_0^1 \left.\frac{\partial \bar{X}}{\partial \bar{X}^{cv}}(\bar{\xi}(s))\right|_{B\rightarrow 2} \left.\frac{\partial \bar{X}^{cv}(s)}{\partial s}\right|_{B\rightarrow 2} ds
\end{aligned} \tag{26}$$

Along each segment of the lower-step integration pathline, one of the parameterized coordinates is held constant, while the other coordinates vary linearly between particle states. Derivatives of the parameterized coordinates are then either the null vector or a finite-difference vector. Along the first pathline segment from State 1 to State B, where $\bar{X}^{cv}$ is held constant, $\partial\bar{\xi}(s)/\partial s = \Delta\bar{\xi}$ and $\partial\bar{X}^{cv}(s)/\partial s = 0$. Alternately, along the second pathline segment from State B to State 2, where $\bar{\xi}$ is held constant, $\partial\bar{\xi}(s)/\partial s = 0$ and $\partial\bar{X}^{cv}(s)/\partial s = \Delta\bar{X}^{cv}$. Along the entire lower-step pathline $\partial\bar{X}(s)/\partial s = \Delta\bar{X}$. Integration of the parameterized total-differential along the lower-step pathline can then be simplified as presented in Equation 27.

$$\int_0^1 \Delta\bar{X}\, ds = \int_0^1 \frac{\partial\bar{X}}{\partial\bar{\xi}}(\bar{\xi}(s), \bar{X}^{cv}(s))\bigg|_{1\to B} \Delta\bar{\xi}\, ds + \int_0^1 \frac{\partial\bar{X}}{\partial\bar{X}^{cv}}(\bar{\xi}(s))\bigg|_{B\to 2} \Delta\bar{X}^{cv}\, ds \qquad (27)$$

The parameterized transformation matrices in Equation 27 are formed by using $\bar{\xi}(s)$ and $\bar{X}^{cv}(s)$ from Equations 23 and 24 in Equations 4, 5, and 9. Solution of Equation 27 is then straightforward, and many discrete-expansions may be obtained. The three discrete-expansions most easily obtained using the lower-step integration pathline are presented in Equation 28.

$$\begin{aligned}
\Delta\bar{X} &= \frac{\partial\bar{X}}{\partial\bar{\xi}}(\hat{\bar{\xi}}, \bar{X}_1^{cv})\,\Delta\bar{\xi} + \frac{\partial\bar{X}}{\partial\bar{X}^{cv}}(\bar{\xi}_2)\,\Delta\bar{X}^{cv} \\
\Delta\bar{X} &= \frac{\partial\bar{X}}{\partial\bar{\xi}}(\bar{\xi}_1, \bar{X}_1^{cv})\,\Delta\bar{\xi} + \frac{\partial^2\bar{X}}{\partial\xi\partial\eta}(\bar{X}_1^{cv})\,\Delta\xi\,\Delta\eta + \frac{\partial\bar{X}}{\partial\bar{X}^{cv}}(\bar{\xi}_2)\,\Delta\bar{X}^{cv} \qquad (28) \\
\Delta\bar{X} &= \frac{\partial\bar{X}}{\partial\bar{\xi}}(\bar{\xi}_2, \bar{X}_1^{cv})\,\Delta\bar{\xi} - \frac{\partial^2\bar{X}}{\partial\xi\partial\eta}(\bar{X}_1^{cv})\,\Delta\xi\,\Delta\eta + \frac{\partial\bar{X}}{\partial\bar{X}^{cv}}(\bar{\xi}_2)\,\Delta\bar{X}^{cv}
\end{aligned}$$

The discrete-expansions obtained using the lower-step integration pathline, Equation 28, are similar to those obtained using the upper-step pathline, Equation 22. The logical-coordinates and cell-vertex coordinates used as arguments within these solutions, however, are defined at opposite particle end-states; these integration pathlines are exact mirror images of each other. Within Equation 28, the cell-vertex arguments for the interpolation derivatives with respect to $\bar{\xi}$, both $\partial\bar{X}/\partial\bar{\xi}$ and $\partial^2\bar{X}/\partial\xi\partial\eta$, are fixed at $\bar{X}_1^{cv}$. Similarly, within Equation 28 the logical-coordinate argument for the geometry-transformation matrix, $\partial\bar{X}/\partial\bar{X}^{cv}$, is fixed at $\bar{\xi}_2$.

Discussion

The eight discrete-expansions presented in this report, listed in Equations 16, 22 and 28, were developed using the new total-differential method. These expansions were developed for

bilinear interpolation defined within quadrilateral cell geometries. In contrast, the existing finite-difference method [73-75] produced only a single discrete-expansion of trilinear interpolation defined within hexahedral cells. Furthermore, the finite-difference expansion is a subset of the total-differential solutions; it is the three-dimensional equivalent of one of the total-differential expansions. For bilinear interpolation, the discrete-expansion that was developed using both the total-differential and the finite-difference methods is repeated in Equation 29.

$$\Delta\bar{X} = \frac{\partial\bar{X}}{\partial\bar{\xi}}(\bar{\xi}_1, \bar{X}_2^{cv})\,\Delta\bar{\xi} + \frac{\partial^2\bar{X}}{\partial\xi\partial\eta}(\bar{X}_2^{cv})\,\Delta\xi\,\Delta\eta + \frac{\partial\bar{X}}{\partial\bar{X}^{cv}}(\bar{\xi}_1)\,\Delta\bar{X}^{cv} \qquad (29)$$

Additional discrete-expansions for interpolation, beyond the eight presented in this report, might be possible using either the total-differential or the finite-difference methods. While the finite-difference method is simple, obtaining an expansion with this technique requires knowledge of the desired solution. In contrast, the integration of a parameterized total-differential is mathematically well founded, and the discrete-expansions for interpolation are obtained without a-priori knowledge of the solution. The total-differential method, therefore, represents a general solution technique for developing discrete-expansions for interpolation.

Particle methods require expansions of interpolation functions for numerical analyses and logical-coordinate evaluation. Application of the discrete-expansions developed herein for these two purposes is beyond the scope of this report. Verification of the new expansions, however, is provided in Appendix A; one of the new discrete-expansions is demonstrated to correctly solve the general problem for two particles located in separate, non-contiguous grid cells. Appendix B presents the total-differential method and discrete-expansions for one-dimensional line elements. Within the following sections, application of the discrete-expansion in Equation 29 for numerical analyses and localization within particle methods is outlined and discussed.

Numerical Analysis

Numerical analysis refers to an analytical investigation of the computational model used to simulate the selected governing equations. The goal of these studies includes establishing the model's consistency and numerical accuracy. Consistency refers to whether a converged solution of the model, an exact solution plus a minimized error term, satisfies the governing equations. Accuracy refers to the model's numerical error, its deviation from an exact solution. Computational verification of a model's accuracy is possible for those limited number of problem types studied; for complex models, this is often the only option available to establish accuracy. Analytical proof of a computational model's consistency and numerical accuracy, valid for all problem types, is preferred but not often included in the literature.

Analytical determination of a particle method's consistency and numerical accuracy are based upon the leading-order error term of the computational model. If this error term approaches zero as the mesh is refined, then the particle method is consistent with the governing equations. The rate at which the leading-order error term vanishes, the convergence rate, is one measure of the model's numerical accuracy. The leading-order error term is evaluated by substituting series expansions for all discrete-terms that appear within the computational model. As previously discussed, particle methods often use interpolation functions within their computational models, but a Taylor's series is not a valid expansion for interpolation. Instead, a discrete-expansion for interpolation is required to complete numerical analyses for these computational models.

For example, reactive particle methods compute trajectories with a velocity interpolated from the discrete solution of the entraining fluid. Numerical analyses of these models requires a discrete-expansion of the velocity-interpolation function, and the expansion must be written relative to a single state, defined here as State 1. Recall that reactive particle trajectories are often computed using multi-step time-integration methods. At any of the intermediate integration steps, the particle's velocity might be evaluated within a separate, non-contiguous grid cell, defined here as State 2. The objective is then to write a general discrete-expansion of the velocity-interpolation function from State 1 to State 2: $\overline{V}_2 = \overline{V}_1 + f(\bar{\xi}, \overline{V}^{cv})$. The discrete-expansion presented in Equation 29 may be rewritten for this purpose as presented in Equation 30.

$$\begin{aligned} \overline{V}(\bar{\xi}_2, \overline{V}_2^{cv}) \;=\; & \overline{V}(\bar{\xi}_1, \overline{V}_1^{cv}) \\ & + \frac{\partial \overline{V}}{\partial \bar{\xi}}(\bar{\xi}_1, \overline{V}_2^{cv})\, \Delta\bar{\xi} \;+\; \frac{\partial^2 \overline{V}}{\partial \xi \partial \eta}(\overline{V}_2^{cv})\, \Delta\xi\, \Delta\eta \;+\; \frac{\partial \overline{V}}{\partial \overline{V}^{cv}}(\bar{\xi}_1)\, \Delta\overline{V}^{cv} \end{aligned} \tag{30}$$

A computational model's leading-order error term is a function of finite-differences of relevant length-scales and other independent variables. For velocity interpolation, these finite-differences are the vectors $\Delta\bar{\xi}$ and $\Delta\overline{V}^{cv}$. A model's leading-order error can only be determined if all terms scaled by these finite-difference vectors are defined at a single state, State 1. The discrete-expansion in Equation 30, however, includes two interpolation derivatives defined with mixed state variables: $\partial\overline{V}(\bar{\xi}_1, \overline{V}_2^{cv})/\partial\bar{\xi}$ and $\partial^2\overline{V}(\overline{V}_2^{cv})/\partial\xi\partial\eta$. Recursive application of Equation 30 can transform the mixed-state interpolated velocity, $\overline{V}(\bar{\xi}_1, \overline{V}_2^{cv})$, into one that is solely dependent upon State 1 variables, $\overline{V}(\bar{\xi}_1, \overline{V}_1^{cv})$. This single-state interpolated velocity can be substituted into Equation 30, and then the numerical analyses of the model may be completed.

For computational models that use interpolation, discrete-expansions represent a key advancement in the capability to both analyze existing models and develop advanced models. For

existing computational models, discrete-expansions provide the capacity to analytically evaluate their consistency and accuracy. Consistency is required and defined objectively; converged solutions of the model either satisfy the governing equations or the model is not consistent. Discrete-expansions, by providing an analytical description of a model's leading-order error term, also provide the capacity to develop advanced computational models. The accuracy of a numerical solution is subjectively pre-determined; simulation fidelity is determined by the model selected and its implementation details. The leading-order error term of an existing model may be used to create a new, advanced computational model that provides greater numerical accuracy.

Logical-Coordinate Evaluation

Logical-coordinate evaluation refers to the spatial-transformation of a position vector from global, physical-space to a local, cell-based coordinate system. Logical-coordinates are often used within interpolation functions to exchange data between particles and discretized continuum-fields. These coordinates are also generally used within localization algorithms to establish a particle's position within the entire discretized domain. Interpolation functions are often used for spatial transformation because they can provide a general relationship between physical and logical coordinates. Discrete-expansions represent the mathematical expression that allows interpolation functions to evaluate a particle's logical-coordinates. The discrete-expansion presented in Equation 29 may be rewritten for this purpose as presented in Equation 31.

$$\frac{\partial \bar{X}}{\partial \bar{\xi}}(\bar{\xi}_1, \bar{X}_2^{cv})\, \Delta\bar{\xi} \;=\; (\bar{X}_2 - \bar{X}_1) - \frac{\partial \bar{X}}{\partial \bar{X}^{cv}}(\bar{\xi}_1)\, \Delta\bar{X}^{cv} \;-\; \frac{\partial^2 \bar{X}}{\partial\xi\partial\eta}(\bar{X}_2^{cv})\, \Delta\xi\, \Delta\eta \qquad (31)$$

The discrete-expansion in Equation 31 is valid between two particles, States 1 and 2, located in separate, non-contiguous grid cells. For logical-coordinate evaluation, the coordinate vectors defined at State 1 are known: $\bar{X}_1$, $\bar{\xi}_1$ and $\bar{X}_1^{cv}$. The only restriction on these vectors is that they must form a consistent set of coordinates as described by the interpolation function: $\bar{X}_1 = \bar{X}(\bar{\xi}_1, \bar{X}_1^{cv})$. The only coordinates known at State 2 are the physical-coordinates of the particle, $\bar{X}_2$. The cell-searching portion of the localization algorithm does, however, identify a guessed cell for the particle at State 2, which provides cell-vertex coordinates, $\bar{X}_2^{cv}$. The only unknown vector is the logical-coordinate vector at State 2, $\bar{\xi}_2$, which is the desired solution.

The interpolation derivatives within Equation 31 are not functions of the solution vector, however, elements of $\bar{\xi}_2$ appear on the right-hand-side of the discrete-expansion. An iterative solution strategy, one that lags the second-order derivative term, can be applied to Equation 31 to obtain the vector, $\Delta\bar{\xi}$. The logical-coordinates at State 2 are then evaluated as $\bar{\xi}_2^{i} = \bar{\xi}_1 + \Delta\bar{\xi}$, where 'i' is an iteration index, and the initial solution guess, $\bar{\xi}_2^{i=0}$, is typically the null vector.

The scalar-multiples of the lagged second-order derivative are defined as $\Delta\xi = \xi_2^{i-1} - \xi_1$ and $\Delta\eta = \eta_2^{i-1} - \eta_1$. The iterative solution of Equation 31 can be monitored with the State 2 difference vector $\Delta\bar{\xi}_2 = \bar{\xi}_2^{i+1} - \bar{\xi}_2^{i}$, and assumed converged when this vector satisfies a tolerance criterion. At convergence, the vectors $\Delta\bar{\xi}$ and $\Delta\bar{X}^{cv}$ are non-zero finite differences.

The most important feature of Equation 31 is that the discrete-expansion is defined between two *fixed* particle positions. State 2 is *absolutely* fixed, invariant throughout the localization problem, by the particle's physical-coordinates, $\bar{X}_2$. Logical-coordinate evaluation completes the definition of State 2 by providing the coordinate vectors $\bar{\xi}_2$ and $\bar{X}_2^{cv}$. In contrast, State 1 is *arbitrarily* fixed; its position within the computational grid is constrained only by the requirement that $\bar{X}_1 = \bar{X}(\bar{\xi}_1, \bar{X}_1^{cv})$. Therefore, a bound $\bar{\xi}_1$ vector may be selected for use within Equation 31 that guarantees a non-singular Jacobian matrix and, thus, an algorithmically robust evaluation method. Furthermore, the solution of Equation 31 for $\bar{\xi}_2$ is computationally efficient; all of its derivatives are constant and only require a single evaluation. Inversion of the Jacobian matrix is then only required once, and it may be reused throughout the iterative solution.

In contrast, existing logical-coordinate evaluation methods, developed from a truncated, single-variable Taylor's series expansion [46,67,69,71,72], are neither robust nor efficient. The most salient feature of these methods is that their expansions are written relative to a *variable* particle position, State 1. While State 2 is absolutely fixed by the particles physical-coordinates, $\bar{X}_2$, State 1 represents an intermediate position within the iterative solution process. These logical-coordinate evaluation methods are not algorithmically robust; if the particle resides outside of the guessed cell and the grid is sufficiently distorted, $\bar{\xi}_1$ is unbound and the Jacobian matrix may become singular, and their iterative solution then fails to converge. Furthermore, these evaluation methods are not computationally efficient; their iterative solution strategy requires the repeated evaluation and inversion of an interpolation derivative, the Jacobian matrix.

The discrete-expansion in Equation 31 represents a general solution method for logical-coordinate evaluation. First, Equation 31 provides a robust and efficient evaluation method that is valid throughout the discretized domain, including between separate, non-contiguous grid cells. Second, if $\bar{X}_2^{cv} = \bar{X}_1^{cv}$ and the higher-order derivative is ignored, the existing evaluation methods may be obtained from Equation 31. Within these methods, the geometry-transformation matrix is nullified since $\Delta\bar{X}^{cv} = 0$, and the Jacobian matrix and the physical-coordinates at State 1 are defined with an intermediate solution vector, $\bar{\xi}_1^{i}$. At convergence, States 1 and 2 are identical: $\bar{\xi}_2 = \bar{\xi}_1$. Finally, if Equation 31 is applied for linear spatial-transformation, such as triangular cell geometries, the Jacobian matrix is constant and the second-order derivative vanishes. Only a single solution of the discrete-expansion is then required to compute a logical-coordinate vector.

Summary

The objective of this research was to develop and verify discrete-expansions for bilinear interpolation defined within quadrilateral cell geometries. Interpolation expansions are required by particle methods for two purposes: numerical analyses used to establish the method's consistency and accuracy, and logical-coordinate evaluation used to locate particles within a grid. Discrete-expansions are similar to multi-variable series expansions but, unlike a Taylor's series, they are valid throughout a discretized domain. Eight discrete-expansions were developed by parametrically integrating the bilinear interpolation functions total-differential between two particles located within separate, non-contiguous cells. This new development method was also applied to one-dimensional interpolation defined within line-elements. A two-dimensional test problem then verified the enhanced capabilities of the new total-differential discrete-expansions.

For any computational model that uses interpolation, discrete-expansions represent a key advancement; they provide the capacity to analytically define a model's leading-order error term and, therefore, establish the mathematical consistency and numerical accuracy of existing models. Discrete-expansions also provide the capacity to develop advanced models; the leading-order error term of an existing model may be used to a create a new model with greater accuracy. Furthermore, one of new discrete-expansions represents a general solution method for evaluating logical-coordinates, which are used to locate particles within a grid. The iterative solution of this expansion, which is valid throughout a discretized domain, is algorithmically robust and computationally efficient. Finally, this discrete-expansion, which may be simplified to obtain the existing evaluation methods, does not require an iterative solution process to compute logical-coordinate vectors for linear spatial-transformation functions.

Acknowledgement

This work was sponsored by the Accelerated Strategic Computing Initiative Program at the Los Alamos National Laboratory. Thanks to Forrest B. Brown, John H. Hall and Stephen R. Lee of the Blanca Project for their support of this investigation. Much thanks to James R. Kamm and Gary L. Sandine of the Applied Physics Division for assistance in this research.

References

1) Watkins, A. P., "Three-Dimensional Modeling of Gas Flow and Sprays in Diesel Engines," *Computer Simulation for Fluid Flow, Heat and Mass Transfer and Combustion in Reciprocating Engines*, Markatos, N. C., Editor, Hemisphere, Washington, D. C., pp. 193-237, 1989.

2) Dukowicz, J. K., "A Particle-Fluid Numerical Model for Liquid Sprays," *Journal of Computational Physics*, Vol. 35, pp. 229-253, 1980.

3) Crowe, C. T., Sharma, M. P. and Stock, D. E., "The Particle-Source-In Cell Model for Gas-Droplet Flows," *Journal of Fluids Engineering*, Vol. 99, pp. 325-331, 1977.

4) Amsden, A. A. and Hirt, C. W., "Yaqui: An Arbitrary Lagrangian-Eulerian Computer Program for Fluid Flow at All Speeds," Los Alamos National Laboratory Report, LA-5100, 1973.

5) O'Rourke, P. J. and Amsden, A. A. "A Particle Numerical Model for Wall Film Dynamics in Port-Injected Engines," SAE Paper 961961, *SAE Transactions*, Vol. 105, pp. 2000-2013, 1996.

6) Nagaoka, M., Kawazoe, H. and Namura, N., "Modeling Fuel Spray Impingement on Hot Wall for Gasoline Engines," SAE Paper 940525, *SAE Transactions*, Vol. 103, pp. 878-896, 1994.

7) Wang, D. M. and Watkins, A. P., "Numerical Modeling of Diesel Spray Wall Impaction Phenomena," *International Journal of Heat and Fluid Flow*, Vol. 14, pp. 301-312, 1993.

8) Naber, J. D. and Reitz, R. D., "Modeling Engine Spray/Wall Impingement," SAE Paper 880107, *SAE Transactions*, Vol. 97, pp. 118-140, 1988.

9) Delnoij, E., Lammers, F. A., Kuipers, J. A. M. and van Swaaij, W. P. M., "Dynamic Simulation of Dispersed Gas-Liquid Two-Phase Flow Using a Discrete Bubble Model," *Chemical Engineering Science*, Vol. 52, pp. 1429-1458, 1997.

10) Sokolichin, A., Eigenberger, G., Lapin, A. and Lubbert, A., "Dynamic Numerical Simulation of Gas-Liquid Two-Phase Flows: Euler/Euler versus Euler/Lagrange," *Chemical Engineering Science*, Vol. 52, pp. 611-626, 1997.

11) Lapin, A. and Lubbert, A., "Numerical Simulation of the Dynamics of Two-Phase Gas-Liquid Flows in Bubble Columns," *Chemical Engineering Science*, Vol. 49, pp. 3661-3674, 1994.

12) Trapp, J. A. and Mortensen, G. A., "A Discrete Particle Model for Bubble-Slug Two-Phase Flows," *Journal of Computational Physics*, Vol. 107, pp. 367-377, 1993.

References Continued

13) Webb, C., Que, F. and Senior, P. R., "Dynamic Simulation of Gas-Liquid Dispersion Behavior in a 2-D Bubble Column Using a Graphics Mini-Supercomputer," *Chemical Engineering Science*, Vol. 47, pp. 3305-3312, 1992.

14) MacCracken, M. C. and Walton, J. J., "The Effects of Interactive Transport and Scavenging of Smoke on the Calculated Temperature Change Resulting from Large Amounts of Smoke," Lawrence Livermore National Laboratory Report, UCRL-91446, 1984.

15) Rider, W. J. and Kothe, D. B., "A Marker Particle Method for Interface Tracking," Los Alamos Laboratory Report LA-UR-95-1740, 1995.

16) Rider, W. J., Kothe, D. B., Mosso, S. J., Cerutti, J. H. and Hochstein, J. I., "Accurate Solution Algorithms for Incompressible Multiphase Flows," AIAA Paper 95-0699, 1995. (Los Alamos Laboratory Report LA-UR-94-3611, 1994.)

17) Gifford, F. A., Barr, S., Malone, R. C. and Mroz, E. J., "Tropospheric Relative Diffusion to Hemispheric Scales," *Atmospheric Environment*, Vol. 22, pp. 1871-1879, 1988.

18) McNider, R. T., Moran, M. D. and Pielke, R. A., "Influence of Diurnal and Inertial Boundary-Layer Oscillations on Long-Range Dispersion," *Atmospheric Environment*, Vol. 22, pp. 2445-2462, 1988.

19) Walton, J. J. and MacCracken, M. C., "Preliminary Report on the Global Transport Model GRANTOUR," Lawrence Livermore National Laboratory Report, UCID-19985, 1984.

20) Hanna, S. R., "Some Statistics of Lagrangian and Eulerian Wind Fluctuations," *Journal of Applied Meteorology*, Vol. 18, pp. 518-525, 1979.

21) Hotchkiss, R. S. and Harlow, F. H., "Air Pollution Transport in Street Canyons," Environmental Protection Agency Report, EPA-R4-73-029, 1973.

22) Hirt, C. W. and Cook, J. L., "Calculating Three-Dimensional Flows Around Structures and Over Rough Terrain," *Journal of Computational Physics*, Vol. 10, pp. 324-340, 1972. (Los Alamos National Laboratory Report LA-DC-13289, 1971.)

23) Hotchkiss, R. S. and Hirt, C. W., "Particulate Transport in Highly Distorted Three-Dimensional Flow Fields," Los Alamos National Laboratory Report LA-DC-72-364, 1972.

References Continued

24) Hotchkiss, R. S., "The Numerical Calculation of Three-Dimensional Flows of Air and Particulates About Structures," Los Alamos National Laboratory Report LA-DC-13071, 1971.

25) Lu, N., "A Semianalytical Method of Path Line Computation for Transient Finite-Difference Groundwater Flow Models," *Water Resources Research*, Vol. 30, pp. 2449-2459, 1994.

26) Schafer-Perini, A. L. and Wilson, J. L., "Efficient and Accurate Front Tracking for Two-Dimensional Groundwater Flow Models," *Water Resources Research*, Vol. 27, pp. 1471-1485, 1991.

27) Tompson, A. F. B. and Gelhar, L. W., "Numerical Simulation of Solute Transport in Three-Dimensional, Randomly Heterogeneous Porous Media," *Water Resources Research*, Vol. 26, pp. 2541-2562, 1990.

28) Goode, D. J., "Particle Velocity Interpolation in Block-Centered Finite Difference Groundwater Flow Models," *Water Resources Research*, Vol. 26, pp. 925-940, 1990.

29) Pollock, D. W., "Semianalytical Computation of Path Lines for Finite-Difference Models," *Ground Water*, Vol. 26, pp. 743-750, 1988.

30) Uffink, G. J. M., "Modeling of Solute Transport with the Random Walk Method," *Groundwater Flow and Quality Modeling*, Custodio, E., Gurgui, A. and Lobo Ferreria, J. P., Editors, D. Reidel Publishing Company, pp. 247-265, 1988.

31) Kinzelbach, W., "The Random Walk Method in Pollutant Transport Simulation," *Groundwater Flow and Quality Modeling*, Custodio, E., Gurgui, A. and Lobo Ferreria, J. P., Editors, D. Reidel Publishing Company, pp. 227-245, 1988.

32) Shafer, J. M., "Reverse Pathline Calculation of Time-Related Capture Zones in Nonuniform Flow," *Ground Water*, Vol. 25, pp. 283-289, 1987.

33) Prickett, T. A., Naymik, T. G. and Lonnquist, C. G., "A Random-Walk Solute Transport Model for Selected Groundwater Quality Evaluations," Bulletin of the Illinois State Water Survey, Vol. 65, pp. 1-104, 1981.

34) Nelson, R. W., "Evaluating the Environmental Consequences of Groundwater Contamination," *Water Resources Research*, Vol. 14, pp. 409-450, 1978.

References Continued

35) Ambegaonkar, A. S., Dhruv, A. S., and Tavlarides, L. L., "Fluid-Particle Hydrodynamics in Agitated Vessels," *Canadian Journal of Chemical Engineering*, Vol. 55, pp. 414-421, 1977.

36) Zeitlin, M. A. and Tavlarides, L. L., "Dispersed Phase Reactor Model for Predicting Conversion and Mixing Effects," *AIChE Journal*, Vol. 18, No. 6, pp. 1268-1271, 1972.

37) Zeitlin, M. A. and Tavlarides, L. L., "Prediction of Mass Transfer Coefficients, Local Concentrations and Binary and Ternary Mass Transfer Rates for Extractors," *Industrial and Engineering Chemistry Process Design and Development*, Vol. 11, No. 4, pp. 532-537, 1972.

38) Zeitlin, M. A. and Tavlarides, L. L., "Fluid-Fluid Interactions and Hydrodynamics in Agitated Dispersions: A Simulation Model," *Canadian Journal of Chemical Engineering*, Vol. 50, pp. 207-215, 1972.

39) Smith, F. G., "A Model of Transient Mixing in a Stirred Tank," *Chemical Engineering Science*, Vol. 52, No. 9, pp. 1459-1478, 1997.

40) Howes, T. and Shardlow, P. J., "Simulation of Mixing in Unsteady Flow Through a Periodically Obstructed Channel," *Chemical Engineering Science*, Vol. 52, No. 7, pp. 1215-1225, 1997.

41) Sobey, I. J., "Dispersion Caused by Separation During Oscillatory Flow Through a Furrowed Channel," *Chemical Engineering Science*, Vol. 40, No. 11, pp. 2129-2134, 1985.

42) Darmofal, D. L. and Haimes, R., "An Analysis of 3D Particle Path Integration Algorithms," *Journal of Computational Physics*, Vol. 123, pp. 182-195, 1996.

43) Cheng, H. P., Cheng, J. R., and Yeh, G. T., "A Particle Tracking Technique for the Lagrangian-Eulerian Finite Element Method in Multi-Dimensions," *International Journal for Numerical Methods in Engineering*, Vol. 39, pp. 1115-1136, 1996.

44) Fairfield, M. S., "Three-Dimensional Visualization of Reactive Flows in Complex Geometries," *High Performance Computing, Grand Challenges in Computer Simulation*, Tentner, A. M., Editor, Simulations Councils, pp. 424-427, 1995. (Los Alamos National Laboratory Report LAUR-95-0251, 1995.)

45) Murman, E. M. and Powell, K. G., "Trajectory Integration in Vortical Flows," *AIAA Journal*, Vol 27, pp. 982-984, 1989.

References Continued

46) Pracht, W. E. and Brackbill, J. U., "BAAL: A Code for Calculating Three-Dimensional Fluid Flows at All Speeds with an Eulerian-Lagrangian Computing Mesh," Los Alamos National Laboratory Report LA-6342, 1976.

47) Wang, J., Kondrashov, D., Liewer, P. C., and Karmesin, S. R., "Three-Dimensional Deformable Grid Electromagnetic Particle-In-Cell for Parallel Computers," *Journal of Plasma Physics*, Vol. 61. pp. 367-389, 1999.

48) Brock, J. S. and Painter, J. W., and Kothe, D. B., "Tracer-Particle Advection: Algorithm Components and Implementation Methods," Los Alamos National Laboratory Report LA-UR-98-5659, 1998.

49) Brock, J. S. and Painter, J. W., "Tracer-Particle Advection: Components, Choices, and a New Alternative," Los Alamos National Laboratory Report LA-UR-98-4691, 1998.

50) Shirayama, S., "Processing of Computed Vector Fields for Visualization," *Journal of Computational Physics*, Vol. 106, pp. 30-41, 1993.

51) Nielson, G. M., Hagen, H. and Muller, H., *Scientific Visualization*, IEEE Computer Society Press, Los Alamitos, CA, 1997.

52) Wolf, R. S. and Yaeger, L., *Visualization of Natural Phenomena*, Springer-Verlag, New York, 1993.

53) Friedhoff, R. M. and Benzon, W., *Visualization: The Second Computer Revolution*, Harry N. Abrams, New York, 1989.

54) Nakayama, T. and Mori, M., "An Eulerian Finite Element Method for Time-Dependent Free Surface Problems in Hydrodynamics," *International Journal for Numerical Methods in Fluids*, Vol. 22, pp. 175-194, 1996.

55) Viecelli. J. A., "A Computing Method for Incompressible Flows Bounded by Moving Walls," *Journal of Computational Physics*, Vol. 8, pp. 119-143, 1971.

56) Amsden, A. A. and Harlow, F. H., "A Simplified MAC Technique for Incompressible Fluid Flow Calculations," *Journal of Computational Physics*, Vol. 6, pp. 322-325, 1970.

References Continued

57) Amsden, A. A. and Harlow, F. H., "The SMAC Method: A Numerical Technique for Calculating Incompressible Fluid Flows," Los Alamos National Laboratory Report LA-4370, 1970.

58) Harlow, F. H. and Welch, J. E., "Numerical Calculation of Time-Dependent Viscous Incompressible Flow of Fluid with Free Surface," *Physics of Fluids*, Vol. 8, pp. 2182-2189, 1965.

59) Welch, J. E., Harlow, F. H., Shannon, J. P. and Daly, B. J., "The MAC Method: A Computing Technique for Solving Viscous, Incompressible, Transient Fluid-Flow Problems Involving Free Surfaces," Los Alamos National Laboratory Report LA-3425, 1965.

60) Tryggvason, G., Bunner, B., Juric, D., Tauber, W., Nas, S., Han, J., Al-Rawahi, N., and Jan, Y., "A Front Tracking Method for the Computations of Multiphase Flow," *Journal of Computational Physics*, Review Paper, Published Spring 2001.

61) Udaykumar, H. S., Kan, H. C., Shyy, W. and Tran-Son-Tay, R., "Multiphase Dynamics in Arbitrary Geometries on Fixed Cartesian Grids," *Journal of Computational Physics*, Vol. 137, pp. 366-405, 1997.

62) Udaykumar, H. S., Shyy, W. and Rao, M. M., "ELAFINT: A Mixed Eulerian-Lagrangian Method for Fluid Flows with Complex and Moving Boundaries," *International Journal for Numerical Methods in Fluids*, Vol. 22, pp. 691-712, 1996.

63) Udaykumar, H. S. and Shyy, W., "A Grid-Supported Marker Particle Scheme for Interface Tracking," *Numerical Heat Transfer*, Part B, Vol. 27, pp. 127-153, 1995.

64) Unverdi, S. O. and Tryggvason, G., "Computations of Multi-Fluid Flows," *Physica D*, Vol. 60, pp. 70-83, 1992.

65) Unverdi, S. O. and Tryggvason, G., "A Front-Tracking Method for Viscous, Incompressible, Multi-Fluid Flows," Journal of Computational Physics, Vol. 100, pp. 25-37, 1992.

66) Miyata, H., "Finite-Difference Simulation of Breaking Waves," *Journal of Computational Physics*, Vol. 65, pp. 179-214, 1986.

67) Allievi, A. and Bermejo, R., "A Generalized Particle-Search Algorithm for Arbitrary Grids," *Journal of Computational Physics*, Vol. 132, pp. 157-166, 1997.

References Continued

68) Lohner, R., "Robust, Vectorized Search Algorithms for Interpolation on Unstructured Grids," *Journal of Computational Physics*, Vol. 118, pp. 380-387, 1995.

69) Westerman, T., "Localization Schemes in 2D Boundary-Fitted Grids," *Journal of Computational Physics*, Vol. 101, pp. 307-313, 1992.

70) Lohner, R. and Ambrosiano, J. "A Vectorized Particle Tracer for Unstructured Grids," *Journal of Computational Physics*, Vol. 91, pp. 22-31, 1990.

71) Wilson, T. L., "LINTERP: A Numerical Algorithm for Interpolating Quadrilateral and Hexahedral Meshes," Los Alamos National Laboratory Report LA-11902-MS, 1990.

72) Brackbill, J. U., and Ruppel, H. M., "FLIP: A Method for Adaptively Zoned, Particle-in-Cell Calculations of Fluid Flows in Two Dimensions," *Journal of Computational Physics*, Vol. 65, pp. 314-343, 1986.

73) Brock, J. S., "A Finite-Difference Logical-Coordinate Evaluation Method For Particle Localization," *Progress of Theoretical Physics*, Sup. 138, pp. 40-42, 2000. (Los Alamos National Laboratory Report LA-UR-99-6493, 1999.)

74) Brock, J. S., "A New Logical-Coordinate Evaluation Method For Particle Localization," Los Alamos National Laboratory Report LA-UR-99-5355, 1999.

75) Brock, J. S., "Comparing Logical-Coordinate Evaluation Methods," Los Alamos National Laboratory Report LA-UR-99-5354, 1999.

76) Wiseman, J. R. and Brock, J. S., "Integrating a Linear Interpolation Function Across Triangular Cell Boundaries," Los Alamos National Laboratory Report LA-UR-00-3330, 2000.

Appendix A: Test Problem

The purpose of this appendix is to verify that the eight discrete-expansions presented in this report, developed for bilinear interpolation using the total-differential method, are valid across quadrilateral cell boundaries. While the following verification has been performed for each expansion in Equations 16, 22 and 28, in this appendix, only one discrete-expansion is used to solve the general problem of two particles located in separate, non-contiguous grid cells. The discrete-expansion selected for this demonstration, originally presented in Equation 16 and repeated in Equation A-1, was obtained using the direct integration pathline.

$$\Delta\overline{X} = \frac{\partial\overline{X}}{\partial\overline{\xi}}(\hat{\overline{\xi}}, \hat{\overline{X}}^{cv})\,\Delta\overline{\xi} + \frac{\partial\overline{X}}{\partial\overline{X}^{cv}}(\hat{\overline{\xi}})\,\Delta\overline{X}^{cv} + \frac{1}{4}\frac{\partial^2\overline{X}}{\partial\xi\partial\eta}(\Delta\overline{X}^{cv})\,\Delta\xi\,\Delta\eta \qquad \text{(A-1)}$$

The test problem selected for this demonstration includes two particles, defined as State 1 and State 2, located in two separate, non-contiguous and non-orthogonal quadrilateral cells; see Figure 4. Recall that a particle's state is defined by a set of physical-coordinates, $\overline{X} = (x, y)^T$, logical-coordinates, $\overline{\xi} = (\xi, \eta)^T$, and cell-vertex coordinates, $\overline{X}^{cv} = ({}^0\overline{X}, {}^1\overline{X}, {}^2\overline{X}, {}^3\overline{X})^T$. The cell-vertex coordinate vector may also be described as $\overline{X}^{cv} = ({}^0x, {}^0y, {}^1x, {}^1y, {}^2x, {}^2y, {}^3x, {}^3y)^T$. The only restriction on the two particle states is that they each form a consistent set of coordinates as described by the bilinear interpolation function: $\overline{X} = \overline{X}(\overline{\xi}, \overline{X}^{cv})$. For the problem shown in Figure 4, the two particle states are defined in Equations A-2 and A-3.

$$\begin{aligned} \text{State 1} \quad : \quad \overline{X}_1 &= (1, 3)^T \\ \overline{\xi}_1 &= (0.179236, 0.579236)^T \\ \overline{X}_1^{cv} &= (0, 0, 5, 0, 6, 6, 0, 5)^T \end{aligned} \qquad \text{(A-2)}$$

$$\begin{aligned} \text{State 2} \quad : \quad \overline{X}_2 &= (12, 6)^T \\ \overline{\xi}_2 &= (0.47590, 0.27590)^T \\ \overline{X}_2^{cv} &= (9, 4, 15, 5, 15, 10, 10, 10)^T \end{aligned} \qquad \text{(A-3)}$$

The discrete-expansion in Equation A-1 includes two first-order interpolation derivatives, the transformation matrices $\partial\overline{X}/\partial\overline{\xi}$ and $\partial\overline{X}/\partial\overline{X}^{cv}$, and one second-order derivative, $\partial^2\overline{X}/\partial\xi\partial\eta$. The second-order derivative is evaluated with the finite-difference vector, $\Delta\overline{X}^{cv}$. In contrast, both transformation matrices in Equation A-1 are evaluated with average logical-coordinates and average cell-vertex coordinates: $\hat{\overline{\xi}} = (\overline{\xi}_1 + \overline{\xi}_2)/2$ and $\hat{\overline{X}}^{cv} = (\overline{X}_1^{cv} + \overline{X}_2^{cv})/2$. For the problem shown in Figure 4, these average vectors are presented in Equation A-4.

$$\begin{aligned}
\text{State Average} \quad : \quad \hat{\bar{\xi}} &= (\hat{\xi}, \hat{\eta})^T \\
&= (0.327568, 0.427568)^T \\
\hat{\bar{X}}^{cv} &= (\hat{{}^0x}, \hat{{}^0y}, \hat{{}^1x}, \hat{{}^1y}, \hat{{}^2x}, \hat{{}^2y}, \hat{{}^3x}, \hat{{}^3y})^T \\
&= (4.5, 2, 10, 2.5, 10.5, 8, 5, 7.5)^T
\end{aligned} \tag{A-4}$$

The first-order interpolation derivatives in Equation A-1 are scaled by the finite-difference vectors $\Delta\bar{\xi}$ and $\Delta\bar{X}^{cv} = (\Delta^0\bar{X}, \Delta^1\bar{X}, \Delta^2\bar{X}, \Delta^3\bar{X})^T$. The second-order interpolation derivative is multiplied by both elements of the logical-coordinate finite-difference vector: $\Delta\xi$ and $\Delta\eta$. For the problem shown in Figure 4, these finite-difference vectors are presented in Equation A-5.

$$\begin{aligned}
\text{State Delta} \quad : \quad \Delta\bar{X} &= (\Delta x, \Delta y)^T = (11, 3)^T \\
\Delta\bar{\xi} &= (\Delta\xi, \Delta\eta)^T = (0.2967, -0.3033)^T \\
\Delta\bar{X}^{cv} &= (\Delta^0 x, \Delta^0 y, \Delta^1 x, \Delta^1 y, \Delta^2 x, \Delta^2 y, \Delta^3 x, \Delta^3 y)^T \\
&= (9, 4, 10, 5, 9, 4, 10, 5)^T
\end{aligned} \tag{A-5}$$

The Jacobian matrix in Equation A-1, $\partial\bar{X}/\partial\bar{\xi}$, was presented in Equation 3 for two-dimensional coordinate transformations. The elements of this matrix were defined in Equations 4 and 5. The geometry-transformation matrix, $\partial\bar{X}/\partial\bar{X}^{cv}$, was presented in Equation 6. The product of this matrix and the finite-difference vector, $\Delta\bar{X}^{cv}$, is presented in Equation A-6.

$$\frac{\partial\bar{X}}{\partial\bar{X}^{cv}}\,\Delta\bar{X}^{cv} = \frac{\partial\bar{X}}{\partial^0\bar{X}}\,\Delta^0\bar{X} + \frac{\partial\bar{X}}{\partial^1\bar{X}}\,\Delta^1\bar{X} + \frac{\partial\bar{X}}{\partial^2\bar{X}}\,\Delta^2\bar{X} + \frac{\partial\bar{X}}{\partial^3\bar{X}}\,\Delta^3\bar{X} \tag{A-6}$$

As previously noted, the non-square geometry-transformation matrix may be partitioned into square sub-matrices: $\partial\bar{X}/\partial^v\bar{X}$ where $v = 0, 1, 2, 3$. The non-zero elements of each diagonal sub-matrix are identical; they are one of the four bilinear interpolation basis functions. Each sub-matrix may then be described as an identity matrix scaled by a basis function. The matrix-vector product in Equation A-6 may then be simplified as presented in Equation A-7.

$$\begin{aligned}
\frac{\partial\bar{X}}{\partial\bar{X}^{cv}}\,\Delta\bar{X}^{cv} &= (1-\xi)\,(1-\eta)\,\Delta^0\bar{X} + (\ \xi\ )\,(1-\eta)\,\Delta^1\bar{X} \\
&\quad + (\ \xi\ )(\ \eta\ )\,\Delta^2\bar{X} + (1-\xi)(\ \eta\ )\,\Delta^3\bar{X}
\end{aligned} \tag{A-7}$$

The second-order interpolation derivative in Equation A-1, $\partial^2\bar{X}/\partial\xi\partial\eta$, is simply a combination of cell-vertex coordinate vectors as presented in Equation A-8.

$$\frac{\partial^2 \bar{X}}{\partial \xi \partial \eta} = {}^0\bar{X} - {}^1\bar{X} + {}^2\bar{X} - {}^3\bar{X} \qquad \text{(A-8)}$$

The bilinear interpolation derivatives and coordinate finite-difference vectors required by each discrete-expansion presented in this report have been defined analytically. The interpolation derivatives were presented as a function of the vectors $\bar{\xi}$ and $\bar{X}^{cv}$. In contrast, the interpolation derivatives in Equation A-1 are evaluated with either the average vectors $\hat{\bar{\xi}}$ and $\hat{\bar{X}}^{cv}$ or the finite-difference vector $\Delta\bar{X}^{cv}$. For the problem shown in Figure 4, these vectors were presented in Equations A-4 and A-5. The algebraic form of Equation A-1 applied to the problem in Figure 4, including matrices, vectors and their products, is presented in Equation A-9.

$$\begin{aligned} \Delta\bar{X} &= \frac{\partial \bar{X}}{\partial \bar{\xi}}(\hat{\bar{\xi}}, \hat{\bar{X}}^{cv})\, \Delta\bar{\xi} + \frac{\partial \bar{X}}{\partial \bar{X}^{cv}}(\hat{\bar{\xi}})\, \Delta\bar{X}^{cv} + \frac{1}{4}\frac{\partial^2 \bar{X}}{\partial \xi \partial \eta}(\Delta\bar{X}^{cv})\, \Delta\xi\, \Delta\eta \\ &= \begin{bmatrix} 5.5 & 0.5 \\ 0.5 & 5.5 \end{bmatrix} \begin{Bmatrix} 0.2967 \\ -0.3033 \end{Bmatrix} + \begin{Bmatrix} 9.4750 \\ 4.4750 \end{Bmatrix} + \frac{1}{4} \begin{Bmatrix} -2 \\ -2 \end{Bmatrix} (0.2967)\, (-0.3033) \\ &= (11, 3)^T \end{aligned} \qquad \text{(A-9)}$$

Equation A-9 correctly predicts the change in particle physical-coordinates between State 1 and State 2: $\Delta\bar{X} = (11, 3)^T$. The symmetry of the Jacobian matrix and the second-order derivative in Equation A-9 is not an inherent feature of discrete-expansions. Instead, this feature is an artifact of the test problem. The simplified system-of-equations does not diminish the test problems appropriateness or this discrete-expansions validity; all terms within Equation A-1 are non-zero and numerous other test problems have been successfully conducted. Therefore, this test problem clearly demonstrates that the eight discrete-expansions presented in this report are valid bilinear interpolation expansions across quadrilateral cell boundaries.

Appendix B: Linear Interpolation

The purpose of this appendix is to develop discrete-expansions for a linear interpolation function defined within line-elements. The following one-dimensional development is nearly identical to the previous development in this report for bilinear interpolation. Discussion of the total-differential method will, therefore, be limited in the following sections. While the bilinear discrete-expansions may be simplified for one-dimensional line-elements, additional expansions for linear interpolation are presented below that are not included in the two-dimensional solutions. Furthermore, the linear discrete-expansions are presented here for completeness; discrete-expansions for bilinear interpolation are presented in this report, and they have been previously reported for trilinear interpolation using the finite-difference method [73-75].

One-dimensional computational space may be discretized into line-elements. Linear functions are generally defined within these elements for data interpolation and spatial transformation. Spatial transformation involves mapping the line-element geometry from a physical, x, to a logical, ξ, coordinate system where $0 \le \xi \le 1$. The one-dimensional interpolation function is linear with respect to both the logical coordinate and the cell-vertex (cv) coordinate vector, $\overline{X}^{cv} = ({}^{0}x, {}^{1}x)^{T}$, as presented in Equation B-1.

$$x(\xi, \overline{X}^{cv}) = (1-\xi)\,{}^{0}x + (\ \xi\ )\,{}^{1}x \tag{B-1}$$

Total Differential

Using the linear function, $x(\xi, \overline{X}^{cv})$, the objective is to establish a relationship between the finite change of the physical coordinate, Δx, the logical coordinate, $\Delta\xi$, and the cell-vertex coordinates, $\Delta\overline{X}^{cv}$. The linear function's total-differential provides a relationship between infinitesimal changes of these vectors, $dx = f(d\xi, d\overline{X}^{cv})$, as presented in Equation B-2.

$$dx = \frac{\partial x(\xi, \overline{X}^{cv})}{\partial \xi}\, d\xi + \frac{\partial x(\xi, \overline{X}^{cv})}{\partial \overline{X}^{cv}}\, d\overline{X}^{cv} \tag{B-2}$$

Logical Coordinate Derivative

The first derivative in the linear interpolation function's total-differential, Equation B-2, represents a coordinate-transformation or Jacobian matrix, $J = \partial x / \partial \xi$. The Jacobian matrix is defined in Equation B-3 for a one-dimensional transformation.

$$\frac{\partial x}{\partial \xi}(\overline{X}^{cv}) = {}^{1}x - {}^{0}x \tag{B-3}$$

Cell-Vertex Coordinate Derivative

The second derivative in the linear interpolation function's total-differential, Equation B-2, represents a geometry-transformation matrix. The matrix structure of $\partial x / \partial \overline{X}^{cv}$, the cell-vertex coordinate derivative, is defined in Equation B-4 for a one-dimensional transformation.

$$\left[\frac{\partial x}{\partial \overline{X}^{cv}} \right]_{1x2} = \left[\frac{\partial x}{\partial^0 x} \quad \frac{\partial x}{\partial^1 x} \right]_{1x2} \tag{B-4}$$

Elements of the geometry-transformation matrix, $\partial x / \partial^0 x$ and $\partial x / \partial^1 x$, are identical to the basis functions used for linear interpolation as presented in Equation B-5.

$$\begin{aligned} \frac{\partial x}{\partial^0 x}(\xi) &= (1 - \xi) \\ \frac{\partial x}{\partial^1 x}(\xi) &= (\quad \xi \quad) \end{aligned} \tag{B-5}$$

The coordinate-transformation matrix, $\partial x(\overline{X}^{cv}) / \partial \xi$, is linear with respect to $\overline{X}^{cv}$. Similarly, the geometry-transformation matrix, $\partial x(\xi) / \partial \overline{X}^{cv}$, is linear with respect to ξ. The linear interpolation function's simplified total-differential is presented in Equation B-6.

$$dx = \frac{\partial x}{\partial \xi}(\overline{X}^{cv})\, d\xi + \frac{\partial x}{\partial \overline{X}^{cv}}(\xi)\, d\overline{X}^{cv} \tag{B-6}$$

Integration Method

The objective is to integrate the linear function's total-differential, Equation B-6, to obtain a discrete-expansion for interpolation: $\Delta x = f(\Delta \xi, \Delta \overline{X}^{cv})$. The limits of integration are two particles located in separate, non-contiguous elements: State 1, $x_1 = x(\xi_1, \overline{X}_1^{cv})$, and State 2, $x_2 = x(\xi_2, \overline{X}_2^{cv})$. Integration of the total-differential is represented in Equation B-7.

$$\int_1^2 dx = \int_1^2 \frac{\partial x}{\partial \xi}(\overline{X}^{cv})\, d\xi + \int_1^2 \frac{\partial x}{\partial \overline{X}^{cv}}(\xi)\, d\overline{X}^{cv} \tag{B-7}$$

The interpolation derivatives, $\partial x / \partial \xi$ and $\partial x / \partial \overline{X}^{cv}$, must both be continuous for the function's total-differential to be valid. While interpolation functions are continuous at the boundaries of adjoining grid elements, the interpolation derivatives are generally not continuous across element boundaries. The linear interpolation function's total-differential is, therefore, not valid between particles located in separate grid elements.

Parameterization

The integration coordinate-space can, however, be parameterized using a linear technique with the variable 's', where $0 \le s \le 1$. The parameterized coordinates, $x(s)$, $\xi(s)$ and $\overline{X}^{cv}(s)$, are then embedded in the interpolation function. The parameterized interpolation derivatives are continuous along the integration pathline. Integration of the parameterized total-differential, with appropriate limits of integration, is represented in Equation B-8.

$$\int_0^1 \frac{\partial x(s)}{\partial s}\, ds = \int_0^1 \frac{\partial x}{\partial \overline{\xi}}(\overline{X}^{cv}(s))\, \frac{\partial \xi(s)}{\partial s}\, ds + \int_0^1 \frac{\partial x}{\partial \overline{X}^{cv}}(\xi(s))\, \frac{\partial \overline{X}^{cv}(s)}{\partial s}\, ds \qquad \text{(B-8)}$$

Solution of Equation B-8 requires definition of an integration pathline between the particle States 1 and 2. Three integration pathlines described within the $(\xi, \overline{X}^{cv})$ plane were selected by this research: direct, upper-step and lower-step integration pathlines.

Direct Integration Pathline

The first integration pathline used to solve Equation B-8 is a straight or direct line between particle States 1 and 2; see Figure 3. The parametrized coordinates, which vary linearly along this direct integration pathline, are presented in Equation B-9.

$$\begin{aligned} 1 \to 2 \quad : \quad x(s) &= (1-s)\, x_1 + (s)\, x_2 \\ \xi(s) &= (1-s)\, \xi_1 + (s)\, \xi_2 \\ \overline{X}^{cv}(s) &= (1-s)\, \overline{X}_1^{cv} + (s)\, \overline{X}_2^{cv} \end{aligned} \qquad \text{(B-9)}$$

Solution of Equation B-8 along the direct integration pathline is represented in Equation B-10, where the interpolation derivatives are appropriately labeled.

$$\begin{aligned} \int_0^1 \left.\frac{\partial x(s)}{\partial s}\right|_{1\to 2} ds &= \int_0^1 \left.\frac{\partial x}{\partial \overline{\xi}}(\overline{X}^{cv}(s))\right|_{1\to 2} \left.\frac{\partial \xi(s)}{\partial s}\right|_{1\to 2} ds \\ &+ \int_0^1 \left.\frac{\partial x}{\partial \overline{X}^{cv}}(\xi(s))\right|_{1\to 2} \left.\frac{\partial \overline{X}^{cv}(s)}{\partial s}\right|_{1\to 2} ds \end{aligned} \qquad \text{(B-10)}$$

Derivatives of the parameterized coordinates are constant finite-difference vectors: $\partial x(s)/\partial s = \Delta x$, $\partial \xi(s)/\partial s = \Delta \xi$, and $\partial \overline{X}^{cv}(s)/\partial s = \Delta \overline{X}^{cv}$. Integration of the parameterized total-differential along the direct pathline can then be simplified as presented in Equation B-11.

$$\int_0^1 \Delta x\, ds = \int_0^1 \left.\frac{\partial x}{\partial \overline{\xi}}(\overline{X}^{cv}(s))\right|_{1\to 2} \Delta \xi\, ds + \int_0^1 \left.\frac{\partial x}{\partial \overline{X}^{cv}}(\xi(s))\right|_{1\to 2} \Delta \overline{X}^{cv}\, ds \qquad \text{(B-11)}$$

The parameterized transformation matrices, $\partial x(\overline{X}^{cv}(s))/\partial\xi$ and $\partial x(\xi(s))/\partial\overline{X}^{cv}$, are formed by substituting $\xi(s)$ and $\overline{X}^{cv}(s)$ from Equation B-9 into Equations B-3 and B-5. These interpolation derivatives are linear with respect to the variable 's'. The three discrete-expansions most easily obtained using the direct integration pathline are presented in Equation B-12.

$$\begin{aligned}
\Delta x &= \frac{\partial x}{\partial\xi}(\hat{\overline{X}}^{cv})\,\Delta\xi + \frac{\partial x}{\partial\overline{X}^{cv}}(\hat{\xi})\,\Delta\overline{X}^{cv} \\
\Delta x &= \frac{\partial x}{\partial\xi}(\overline{X}_1^{cv})\,\Delta\xi + \frac{\partial x}{\partial\xi}(\Delta\overline{X}^{cv})\,\Delta\xi + \frac{\partial x}{\partial\overline{X}^{cv}}(\xi_1)\,\Delta\overline{X}^{cv} \\
\Delta x &= \frac{\partial x}{\partial\xi}(\overline{X}_2^{cv})\,\Delta\xi - \frac{\partial x}{\partial\xi}(\Delta\overline{X}^{cv})\,\Delta\xi + \frac{\partial x}{\partial\overline{X}^{cv}}(\xi_2)\,\Delta\overline{X}^{cv}
\end{aligned} \qquad \text{(B-12)}$$

The first discrete-expansion in Equation B-12 is the one-dimensional equivalent of the direct-pathline bilinear expansions in Equation 16. The remaining two discrete-expansions in Equation B-12 are unique to linear interpolation. These expansions include coordinate and geometry-transformation matrices that are both evaluated at either State 1 or State 2. An additional Jacobian matrix, evaluated with the cell-vertex coordinate finite-difference vector, $\Delta\overline{X}^{cv}$, then appears as a correction factor for the single-state transformation matrices.

Upper-Step Integration Pathline

The second integration pathline used to solve Equation B-8 is comprised of two line-segments between particle States 1 and 2 that form an upper-step within the $(\xi, \overline{X}^{cv})$ plane. The first pathline segment is a line of constant ξ from State 1 to State A; see Figure 3. The second pathline segment is a line of constant $\overline{X}^{cv}$ from State A to State 2. The parameterized coordinates for the upper-step integration pathline are presented in Equations B-13 and B-14.

$$\begin{aligned}
1 \rightarrow A \quad : \quad x(s) &= (1-s)\,x_1 + (s)\,x_A \\
\xi(s) &= (1-s)\,\xi_1 + (s)\,\xi_A \;;\; \xi_A = \xi_1 \\
&= \xi_1 \\
\overline{X}^{cv}(s) &= (1-s)\,\overline{X}_1^{cv} + (s)\,\overline{X}_A^{cv} \;;\; \overline{X}_A^{cv} = \overline{X}_2^{cv} \\
&= (1-s)\,\overline{X}_1^{cv} + (s)\,\overline{X}_2^{cv}
\end{aligned} \qquad \text{(B-13)}$$

$$
\begin{aligned}
A \rightarrow 2 \quad : \quad x(s) &= (1-s)\, x_A + (s)\, x_2 \\
\xi(s) &= (1-s)\, \xi_A + (s)\, \xi_2 \;\; ; \;\; \xi_A = \xi_1 \\
&= (1-s)\, \xi_1 + (s)\, \xi_2 \\
\overline{X}^{cv}(s) &= (1-s)\, \overline{X}^{cv}_A + (s)\, \overline{X}^{cv}_2 \;\; ; \;\; \overline{X}^{cv}_A = \overline{X}^{cv}_2 \\
&= \overline{X}^{cv}_2
\end{aligned}
\tag{B-14}
$$

Solution of Equation B-8 along the upper-step integration pathline is represented in Equation B-15, where the interpolation derivatives are appropriately labeled.

$$
\begin{aligned}
&\int_0^1 \frac{\partial x(s)}{\partial s}\bigg|_{1\rightarrow A} ds + \int_0^1 \frac{\partial x(s)}{\partial s}\bigg|_{A\rightarrow 2} ds = \\
&+ \int_0^1 \frac{\partial x}{\partial \overline{\xi}}(\overline{X}^{cv}(s))\bigg|_{1\rightarrow A} \frac{\partial \xi(s)}{\partial s}\bigg|_{1\rightarrow A} ds + \int_0^1 \frac{\partial x}{\partial \overline{\xi}}(\overline{X}^{cv}(s))\bigg|_{A\rightarrow 2} \frac{\partial \xi(s)}{\partial s}\bigg|_{A\rightarrow 2} ds \\
&+ \int_0^1 \frac{\partial x}{\partial \overline{X}^{cv}}(\xi(s))\bigg|_{1\rightarrow A} \frac{\partial \overline{X}^{cv}(s)}{\partial s}\bigg|_{1\rightarrow A} ds + \int_0^1 \frac{\partial x}{\partial \overline{X}^{cv}}(\xi(s))\bigg|_{A\rightarrow 2} \frac{\partial \overline{X}^{cv}(s)}{\partial s}\bigg|_{A\rightarrow 2} ds
\end{aligned}
\tag{B-15}
$$

Along the first segment of the upper-step pathline from State 1 to State A, where ξ is constant, $\partial\xi(s)/\partial s = 0$ and $\partial\overline{X}^{cv}(s)/\partial s = \Delta\overline{X}^{cv}$. Alternately, along the second pathline segment from State A to State 2, where $\overline{X}^{cv}$ is constant, $\partial\xi(s)/\partial s = \Delta\xi$ and $\partial\overline{X}^{cv}(s)/\partial s = 0$. Along the entire pathline $\partial x(s)/\partial s = \Delta x$. Integration of the parameterized total-differential along the upper-step pathline can then be simplified as presented in Equation B-16.

$$
\int_0^1 \Delta x\, ds = \int_0^1 \frac{\partial x}{\partial \overline{\xi}}(\overline{X}^{cv}(s))\bigg|_{A\rightarrow 2} \Delta\xi\, ds + \int_0^1 \frac{\partial x}{\partial \overline{X}^{cv}}(\xi(s))\bigg|_{1\rightarrow A} \Delta\overline{X}^{cv}\, ds \tag{B-16}
$$

The parameterized transformation matrices are formed by substituting $\xi(s)$ and $\overline{X}^{cv}(s)$ from Equations B-13 and B-14 into Equations B-3 and B-5. These interpolation derivatives are linear with respect to the variable ‘s’. The single discrete-expansion most easily obtained using the upper-step integration pathline is presented in Equation B-17.

$$
\Delta x = \frac{\partial x}{\partial \overline{\xi}}(\overline{X}^{cv}_2)\, \Delta\xi + \frac{\partial x}{\partial \overline{X}^{cv}}(\xi_1)\, \Delta\overline{X}^{cv} \tag{B-17}
$$

The discrete-expansion in Equation B-17 is the one-dimensional equivalent of the upper-step-pathline bilinear expansions in Equation 22. This expansion is also the one-dimensional equivalent of the discrete-expansion obtained with the existing finite-difference method [73-75].

Therefore, the total-differential and finite-difference methods of developing discrete-expansions produce identical results for similar computational cell geometries.

Lower-Step Integration Pathline

The third integration pathline used to solve Equation B-8 is comprised of two line-segments between particle States 1 and 2 that form a lower-step within the $(\xi, \overline{X}^{cv})$ plane. The first pathline segment is a line of constant $\overline{X}^{cv}$ from State 1 to State B; see Figure 3. The second pathline segment is a line of constant ξ from State B to State 2. The parameterized coordinates for the lower-step integration pathline are presented in Equations B-18 and B-19.

$$
\begin{aligned}
1 \rightarrow B \quad : \quad x(s) &= (1-s)\, x_1 + (s)\, x_B \\
\xi(s) &= (1-s)\, \xi_1 + (s)\, \xi_B \;;\; \xi_B = \xi_2 \\
&= (1-s)\, \xi_1 + (s)\, \xi_2 \\
\overline{X}^{cv}(s) &= (1-s)\, \overline{X}_1^{cv} + (s)\, \overline{X}_B^{cv} \;;\; \overline{X}_B^{cv} = \overline{X}_1^{cv} \\
&= \overline{X}_1^{cv}
\end{aligned}
\tag{B-18}
$$

$$
\begin{aligned}
B \rightarrow 2 \quad : \quad x(s) &= (1-s)\, x_B + (s)\, x_2 \\
\xi(s) &= (1-s)\, \xi_B + (s)\, \xi_2 \;;\; \xi_B = \xi_2 \\
&= \xi_2 \\
\overline{X}^{cv}(s) &= (1-s)\, \overline{X}_B^{cv} + (s)\, \overline{X}_2^{cv} \;;\; \overline{X}_B^{cv} = \overline{X}_1^{cv} \\
&= (1-s)\, \overline{X}_1^{cv} + (s)\, \overline{X}_2^{cv}
\end{aligned}
\tag{B-19}
$$

Solution of Equation B-8 along the lower-step integration pathline is represented in Equation B-20, where the interpolation derivatives are appropriately labeled.

$$
\begin{aligned}
&\int_0^1 \left.\frac{\partial x(s)}{\partial s}\right|_{1\rightarrow B} ds + \int_0^1 \left.\frac{\partial x(s)}{\partial s}\right|_{B\rightarrow 2} ds = \\
&+ \int_0^1 \left.\frac{\partial x}{\partial \overline{\xi}}(\overline{X}^{cv}(s))\right|_{1\rightarrow B} \left.\frac{\partial \xi(s)}{\partial s}\right|_{1\rightarrow B} ds + \int_0^1 \left.\frac{\partial x}{\partial \overline{\xi}}(\overline{X}^{cv}(s))\right|_{B\rightarrow 2} \left.\frac{\partial \xi(s)}{\partial s}\right|_{B\rightarrow 2} ds \\
&+ \int_0^1 \left.\frac{\partial x}{\partial \overline{X}^{cv}}(\xi(s))\right|_{1\rightarrow B} \left.\frac{\partial \overline{X}^{cv}(s)}{\partial s}\right|_{1\rightarrow B} ds + \int_0^1 \left.\frac{\partial x}{\partial \overline{X}^{cv}}(\xi(s))\right|_{B\rightarrow 2} \left.\frac{\partial \overline{X}^{cv}(s)}{\partial s}\right|_{B\rightarrow 2} ds
\end{aligned}
\tag{B-20}
$$

Along the first segment of the lower-step pathline from State 1 to State B, where $\overline{X}^{cv}$ is constant, $\partial\xi(s)/\partial s = \Delta\xi$ and $\partial\overline{X}^{cv}(s)/\partial s = 0$. Alternately, along the second pathline segment from State B to State 2, where ξ is constant, $\partial\xi(s)/\partial s = 0$ and $\partial\overline{X}^{cv}(s)/\partial s = \Delta\overline{X}^{cv}$. Along the

entire pathline $\partial x(s)/\partial s = \Delta x$. Integration of the parameterized total-differential along the lower-step pathline can then be simplified as presented in Equation B-21.

$$\int_0^1 \Delta x \, ds = \int_0^1 \frac{\partial x}{\partial \xi}(\bar{X}^{cv}(s))\Big|_{1 \to B} \Delta\xi \, ds + \int_0^1 \frac{\partial x}{\partial \bar{X}^{cv}}(\xi(s))\Big|_{B \to 2} \Delta\bar{X}^{cv} \, ds \qquad \text{(B-21)}$$

The parameterized transformation matrices are formed by substituting $\xi(s)$ and $\bar{X}^{cv}(s)$ from Equations B-18 and B-19 into Equations B-3 and B-5. These interpolation derivatives are linear with respect to the variable 's'. The single discrete-expansion most easily obtained using the lower-step integration pathline is presented in Equation B-22.

$$\Delta x = \frac{\partial x}{\partial \xi}(\bar{X}_1^{cv}) \, \Delta\xi + \frac{\partial x}{\partial \bar{X}^{cv}}(\xi_2) \, \Delta\bar{X}^{cv} \qquad \text{(B-22)}$$

The discrete-expansion in Equation B-22 is the one-dimensional equivalent of the lower-step-pathline bilinear expansions in Equation 28. The discrete-expansions for linear interpolation obtained with the upper-step and lower-step pathlines, Equations B-17 and B-22, are nearly identical. While the form of these expansions are identical, the interpolation derivatives are evaluated at opposite particle end-states; these pathlines are exact mirror images of each other.

Recall that the derivatives of the linear interpolation function are linear with respect to both the logical-coordinate and cell-vertex coordinate vectors. The transformation matrices are then easily manipulated, allowing other forms of the discrete-expansions than those presented in Equations B-12, B-17, and B-22. The second expansion in Equation B-12, obtained using the direct pathline, is equivalent to the upper-step expansion in Equation B-17. Similarly, the third expansion in Equation B-12 is equivalent to the lower-step expansion in Equation B-22.

Discussion

For linear interpolation, Taylor's series are not valid expansions across line-element boundaries. In contrast, the discrete-expansions in Equation B-12, B-17, and B-22 acknowledge the full functional dependence of interpolation and account for mapping discontinuities across element boundaries. These expansions are, therefore, valid for numerical analyses. For logical-coordinate evaluation, both the existing method and a new method based on the upper-step discrete-expansion are algorithmically robust; the one-dimensional Jacobian matrix is not a function of the unknown logical coordinate. The existing method does, however, still require an iterative solution strategy for spatial-transformation. In contrast, the new evaluation method is computationally efficient; Equation B-17 can be solved directly for logical-coordinate evaluation.

Figures

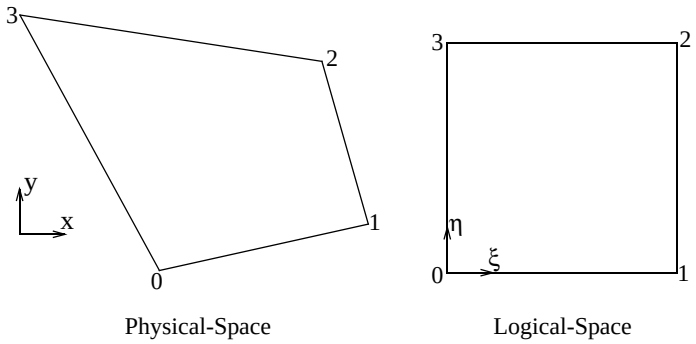

Figure 1: Coordinate Transformation

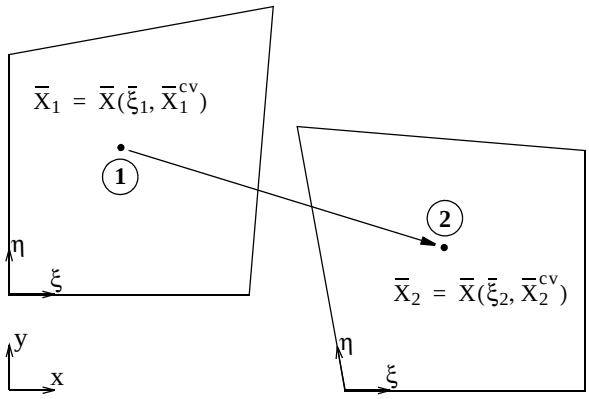

Figure 2: Limits of Integration

Figures Continued

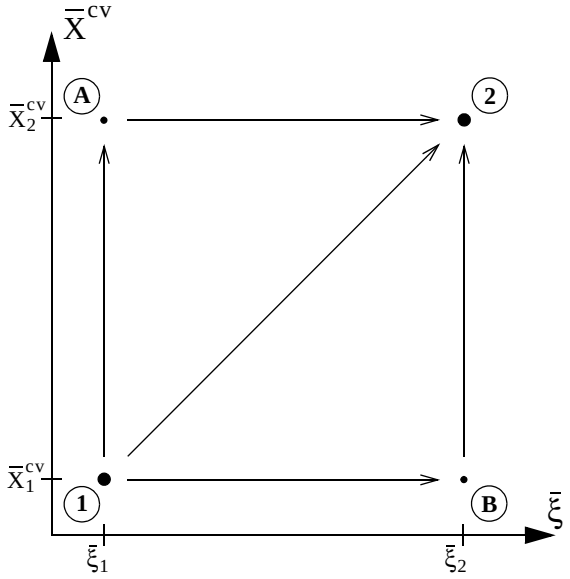

Figure 3: Integration Pathlines

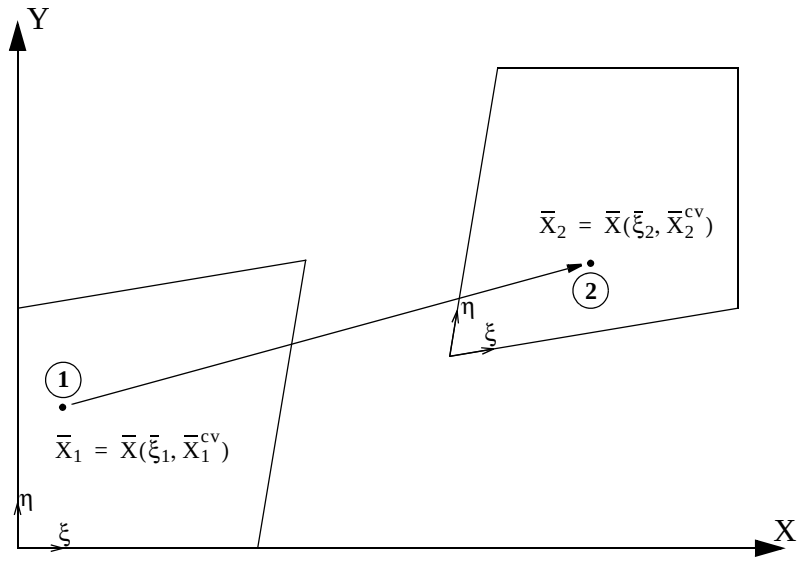

Figure 4: Example Problem Geometry